Columbia preprint CU–TP–639

Perturbative versus Lattice QCD Energy Density Correlators at High Temperatures[†]

Dirk H. Rischke[‡] and Miklos Gyulassy

Physics Department, Pupin Physics Laboratories, Columbia University
538 W 120th Street, New York, NY 10027, U.S.A.

August 1994

Abstract

Correlators of magnetic and electric field energy density are investigated for SU(N_c) gauge theory at high temperatures T. At separations $z \leq 2/T$ the correlators are shown to be dominated by a power–law behavior even for finite gluon screening masses. This continuum behavior is well approximated on current 4×16^3–lattices in the perturbative limit and leads to a considerable overestimate of screening masses deduced from fitting the lattice correlators with conventional exponential forms. The use of extended sources and sinks to enhance the signal improves the situation for screening masses $m \gg T$ but leads to a largely uncontrolled error for masses less than T. In fact, we show that recent lattice QCD data of Grossmann et al., from which a magnetic screening mass $m_M \approx 2.9\,T$ was deduced, may even be consistent with a vanishing actual magnetic screening mass.

[†] This work was supported by the Director, Office of Energy Research, Division of Nuclear Physics of the Office of High Energy and Nuclear Physics of the U.S. Department of Energy under Contract No. DE-FG-02-93ER-40764.

[‡]Partially supported by the Alexander von Humboldt–Stiftung under the Feodor–Lynen program.

1 Introduction and Conclusions

In a recent lattice QCD study of SU(3) pure gauge theory [1] the plaquette–plaquette correlation functions were measured at high temperatures. Below the deconfinement transition temperature ($T_c \sim 200$ MeV) the observed exponential fall–off of those correlators was used to determine the mass spectrum of glueballs. Above T_c the two lowest masses deduced from the decay of the correlators were interpreted as twice the electric and magnetic screening mass in the gluon plasma. The interesting result reported in [1] that we focus on is the claim that just above the critical temperature, $T \approx 1.5\,T_c$, the magnetic screening mass, $m_M/T \approx 2.9 \pm 0.2$, is apparently twice as large as the electric screening mass, $m_E/T \approx 1.4 \pm 0.2$. Our interest in these results stems from the sensitivity of certain transport properties and hence signatures of quark–gluon plasmas produced in ultrarelativistic nuclear collisions [2, 3] to the ratio of these screening masses. In Ref. [4] it was shown that the color relaxation time in a plasma is

$$t_c = [3\alpha_s T f(m_E/m_M)]^{-1} \; , \tag{1}$$

where $f(x) \approx \log(x)$ as $x \to \infty$. This time scale controls the lifetime of collective color excitations in the plasma such as the plasmon. Also next–to–leading–order corrections to the electric screening mass depend self–consistently on the ratio m_E/m_M [5]. In lowest order perturbation theory, $m_E/T = g[(N_c + N_f/2)/3]^{1/2}$ while $m_M/T = 0$ [6]. The infrared magnetic singularities in higher orders are however expected [7] to produce a non–perturbative $m_M/T \sim g^2$. In the weak–coupling limit ($T \gg T_c$), $m_E/m_M \sim 1/g \gg 1$, and there is a natural ordering of the screening scales, $T \gg gT \gg g^2T$. However, at $T \approx 1.5\,T_c$, $m_E/m_M \approx 1/2$ [1], and the measured screening masses imply a reversal of that perturbative ordering. Since the temperatures accessible via nuclear collisions are of the order of $2\,T_c$, this inverse ordering of screening scales could have important phenomenological implications. For example, it implies a higher color conductivity which in turn could decrease the produced transverse energy and the dilepton rate [8].

The screening masses are also of general interest as another test of the viability of the perturbative picture of the quark–gluon plasma. On the one hand, the lattice entropy density [9], color electric screening mass [10], baryon susceptibility [11], and spatial dependence of higher mass meson and baryon correlators [12] are all consistent with the perturbative picture of the quark–gluon plasma, even near T_c. On the other hand, the temperature dependence of the energy density and pressure deviate strongly from the ideal Stephan–Boltzmann behavior up to several times T_c [13, 14, 15], the decay of the scalar and pseudoscalar meson correlation functions cannot be reconciled with free propagation of the $q\bar{q}$–pair [12], and $q\bar{q}$–wavefunctions behave as if the quarks were strongly bound [16].

The recent measurement [1] of $m_M \approx 2\,m_E$ poses a further problem for the perturbative picture of the gluon plasma. How can static color magnetic fields be screened on such a small distance scale? In a magnetic screening volume $4\pi/(3m_M^3)$ there is less than 1/2 gluon on the average in the perturbative picture. Non–perturbative mechanisms, such as a very dense color magnetic monopole gas, would have to exist to account for that large a magnetic screening mass. However, there appears to be no consistent effective QCD action that could

generate such a monopole gas [17].

In this work we aim to clarify how the lattice results of [1] above T_c may translate into continuum physics. To this end we assume that the lattice spacing is small enough to allow the plaquette correlators to be related to energy density correlators. The latter can be decomposed into multi–gluon exchange diagrams. We furthermore assume that the dominant contribution is given by the exchange of two dressed gluons. According to standard arguments, this would give rise to a decay of the correlator governed by twice the gluon screening mass, in agreement with the interpretation the authors of [1] have provided for their results. We first investigate the two–gluon exchange diagram in the interaction–free case to provide better insight on the screened case to be discussed subsequently. For distances $z \ll 1/T$, i.e., on momentum scales where temperature effects are negligible, the correlators behave $\sim z^{-5}$, as expected from dimensional arguments. For $z \geq 1/2T$ this behavior is changed to a decay $\sim z^{-4}$ due to finite temperature effects. Then we study the effect of self–energy insertions. We show that the structure of the electric correlator is considerably more complex than that of the magnetic since the former mixes the longitudinal and transverse polarization effects. In both cases, for $z \leq 2/T$ the correlators are found to be dominated by the power–law behavior encountered in the interaction–free case and not by the exponential decay expected for gluons with a finite screening mass.

We then calculate the correlators on a lattice in the weak–coupling limit and show that the continuum limit is well approximated on a 4×16^3–lattice. Consequently, the power–law behavior is still prominent [18] and leads to an overestimate of the masses deduced from conventional exponential–type fit functions. The power–law behavior is caused by the point source and sink of the correlator. However, in [1] fuzzed links [19] were used which have the effect of "smearing" out the sources and sinks and partially remove the power–law enhancement at small distances. We introduce a model for fuzzed links which incorporates the smearing and show that the relative residual error in determining the screening masses indeed becomes small if the latter are large compared to T. However, for a *vanishing* screening mass this fuzzing model still leads to an apparent *finite* mass. In fact, we show that the current lattice data [1] may even be consistent with a vanishing magnetic screening mass ! The screening masses obtained from energy density correlators are therefore inconclusive and require confirmation from an independent measurement of e.g. the gluon propagator [20].

The remaining sections are organized as follows. In Section 2 we review in more detail the results of Ref. [1] and relate them to our investigations. In Section 3 the energy density correlators are decomposed in terms of multi–gluon exchange. Section 4 comprises a discussion of the interaction–free case. In Section 5 we discuss the correlators for dressed gluons. Section 6 is devoted to the transcription of the perturbative continuum results onto the lattice. In Section 7 we investigate a model for fuzzed links and their effect on the extraction of screening masses.

We use natural units $\hbar = c = 1$ and, except for Section 6 and 7, the Minkowski metric $g^{\mu\nu} = \mathrm{diag}(+,-,-,-)$. This implies $x^\mu = (-i\tau, \mathbf{x})$ and $k^\mu = (-i\omega_n, \mathbf{k})$, with the gluonic Matsubara frequencies $\omega_n = 2\pi n T$.

2 Plaquette correlators in lattice QCD

In the perturbative picture of a quark–gluon plasma as a weakly interacting system, $q\bar{q}$–(or meson) correlators are essentially given by a single $q\bar{q}$–loop, since the mutual interaction between the quark and the antiquark is screened by the hot environment. Also, a quark acquires a dynamical mass $m_q \sim gT$ [21]. The correlator is roughly proportional to the square of the (dressed) quark propagator [22]. For (large) spatial distances, the decay of the latter is governed by the lowest fermionic "energy" $[(\pi T)^2 + m_q^2]^{1/2}$ (πT being the smallest fermionic Matsubara frequency). Since $\pi^2 \gg g^2$ we may neglect the quark mass as compared to the Matsubara frequency [23] and the spatial meson correlator decays like $\exp\{-2\pi z T\}$ [24]. After correcting for lattice artefacts, the lattice data for vector and axial vector meson are found to be in good agreement with this picture [12]. The scalar/pseudoscalar channel is, however, an important exception in that it only decays $\sim \exp\{-\pi z T\}$. This points towards a strong residual interaction in this channel, see e.g. [25, 26].

However, as the study of $q\bar{q}$–wavefunctions has revealed [16], *even* in the vector channel the quark–antiquark pair may be strongly bound. The reason why the corresponding binding energy does not show up in the mass extracted from the correlator is the same why we could neglect the quark mass in our above consideration: it is negligible as compared to $2\pi T$ which originates from the lowest fermionic Matsubara frequency [16]. It is therefore difficult to extract either the residual interaction effects or dynamical quark masses from spatial $q\bar{q}$–correlation functions [27].

In view of this, the study of glueballs is of special interest: since the lowest Matsubara frequency for gluons is zero, the measurement of glueball correlators is not impaired by the above mentioned effect. They may thus provide more detailed information on residual interactions and the gluon screening mass. In [1] the irreducible representations for the glueball states on the lattice were identified and their masses measured via the decay of the corresponding spatial correlation functions [18]. It was found that above T_c the lowest mass state no longer corresponds to a glueball with definite quantum numbers. Rather, it belongs to the (connected) correlator between plaquette operators of the form

$$P_t \equiv P_{0x} + P_{0y} \ , \tag{2}$$

where

$$P_{0i} = \frac{1}{2N_c} \ \mathrm{Tr} \left[U_0 U_i U_0^\dagger U_i^\dagger \right]$$

is the elementary temporal plaquette with two spatial links U_i and two temporal links U_0,

$$U_\mu = \exp\left\{ iga\mathcal{A}_\mu \right\} \ ,$$

with $\mathcal{A}_\mu \equiv A_\mu^b G^b$, and the generators of $\mathrm{SU}(N_c)$ G^b, $b = 1, ..., N_c^2 - 1$. The lattice spacing a is a dynamical quantity in the sense that it decreases with decreasing coupling g according to the QCD β–function [28]. Since g decreases with increasing temperature, at sufficiently high T the lattice spacing should be small enough to permit an expansion of the plaquette operator in powers of a. To lowest (non–trivial) order [29] in a, the plaquette operator (2)

is therefore proportional to

$$P_t \sim \mathrm{Tr}\left[\mathcal{E}_x^2 + \mathcal{E}_y^2\right] \ , \tag{3}$$

where $\mathcal{E}_i \equiv \mathcal{F}_{i0} = F_{i0}^b G^b = E_i^b G^b$ is the ith component of the electric field strength ($\mathcal{F}_{\mu\nu}$ is the field–strength tensor). Thus, (2) is proportional to the color electric field energy density. As will be shown in detail in Section 3, the field energy density correlator can be decomposed in terms of multi–gluon exchange diagrams, the simplest of which is a one–loop, two–gluon exchange diagram. In the perturbative picture of the gluon plasma, this diagram is expected to give the dominant contribution to the energy density correlator, since mutual interactions between gluons are screened by the hot environment. In Section 5 we will show that in this case the mass determining the exponential decay of the energy density correlator is twice the gluon screening mass. It was found in [1] that the mass extracted from the correlator between the P_t is consistent with the mass extracted from the Polyakov–loop correlation function, which for $T \approx 1.5\,T_c$ agrees well with the perturbative result $2\,m_E$. This suggests that indeed the perturbative picture of the gluon plasma is valid, i.e., that the one–loop, two–gluon exchange diagram constitutes the dominant contribution to the P_t–correlator at $T \approx 1.5\,T_c$. In our following continuum analysis, this will be our main working *assumption*. However, we emphasize that there is no rigorous proof that the respective temperature $T \approx 1.5\,T_c$ is sufficiently high and, consequently, the lattice spacing a sufficiently small so that the energy density correlators accurately reflect the plaquette correlators, and that the dominant contribution to the energy density correlators is the one–loop, two–gluon exchange.

The second lowest mass extracted from the spectrum of all glueball–like excitations above T_c was identified to belong essentially to the connected correlator between elementary spatial plaquettes

$$P_s \equiv P_{xy} \ , \tag{4}$$

which, to lowest non–trivial order in a, are proportional to the magnetic field energy density in z–direction:

$$P_s \sim \mathrm{Tr}\ \mathcal{B}_z^2 \ , \tag{5}$$

$\mathcal{B}_z \equiv \mathcal{F}_{xy} = F_{xy}^b G^b = B_z^b G^b$. In analogy to the electric correlator, the authors of [1] interpreted this screening mass as twice the non–perturbative magnetic screening mass m_M.

3 Energy density correlators in terms of multi–gluon exchange

As indicated in the last section, if one assumes that the dominant contribution to the energy density correlators is given by two–gluon exchange, then this allows an interpretation of the mass determined from the decay of the correlators as twice the gluon screening mass. In order to clarify this, we decompose the energy density correlators into multi–gluon exchange diagrams. We start with the magnetic correlator which has the simpler structure. The magnetic point–to–point correlator between $r \equiv (-i\tau, \mathbf{x})$ and $r' \equiv (-i\tau', \mathbf{x}')$ reads

$$M(r, r') \ \equiv \ \left\langle \mathrm{Tr}\ \mathcal{B}_z^2(r)\ \mathrm{Tr}\ \mathcal{B}_z^2(r') \right\rangle_c$$

$$\equiv \quad \mathrm{Tr}[G^a G^b]\ \mathrm{Tr}[G^c G^d]\ \left\langle F^a_{xy}(r) F^b_{xy}(r) F^c_{xy}(r') F^d_{xy}(r') \right\rangle_c \ . \tag{6}$$

The subscript "c" at the ensemble average brackets indicates that only the connected part of the respective expression is to be taken into account. Each color trace yields a factor 1/2 and a Kronecker delta in the color indices. Inserting the definition of the non–Abelian field strength

$$F^a_{\mu\nu} \equiv \partial_\mu A^a_\nu - \partial_\nu A^a_\mu - g f^{abc} A^b_\mu A^c_\nu \ ,$$

we arrive at the following decomposition

$$M(r,r') \equiv M^{(0)}(r,r') + g^2\ M^{(1)}(r,r') + g^4\ M^{(2)}(r,r') \tag{7}$$

with

$$M^{(0)}(r,r') \ = \ \frac{1}{4} \left\langle \left[\partial_x A^a_y(r) - \partial_y A^a_x(r)\right]^2 \left[\partial_{x'} A^b_y(r') - \partial_{y'} A^b_x(r')\right]^2 \right\rangle_c \ , \tag{8}$$

$$\begin{aligned} M^{(1)}(r,r') \ = \ & \frac{1}{4} f^{acd} f^{aef} \left\{ \left\langle \left[\partial_x A^b_y(r) - \partial_y A^b_x(r)\right]^2 A^c_x(r') A^d_y(r') A^e_x(r') A^f_y(r') \right\rangle_c \right. \\ & \left. + \left\langle \left[\partial_{x'} A^b_y(r') - \partial_{y'} A^b_x(r')\right]^2 A^c_x(r) A^d_y(r) A^e_x(r) A^f_y(r) \right\rangle_c \right\} \end{aligned} \tag{9}$$

$$+\ f^{acd} f^{bef} \ \left\langle \left[\partial_x A^a_y(r) - \partial_y A^a_x(r)\right] A^c_x(r) A^d_y(r) \left[\partial_{x'} A^b_y(r') - \partial_{y'} A^b_x(r')\right] A^e_x(r') A^f_y(r') \right\rangle_c \ ,$$

$$M^{(2)}(r,r') \ = \ \frac{1}{4}\ f^{acd} f^{agh} f^{bef} f^{bij} \left\langle A^c_x(r) A^d_y(r) A^g_x(r) A^h_y(r) A^e_x(r') A^f_y(r') A^i_x(r') A^j_y(r') \right\rangle_c \tag{10}$$

In order to calculate the ensemble averages we Fourier–transform the gluon fields according to

$$A^a_\mu(r) = \frac{1}{\sqrt{TV}} \sum_k e^{-ik\cdot r} A^a_\mu(k) \ . \tag{11}$$

The normalization makes the Fourier amplitudes $A^a_\mu(k)$ dimensionless numbers. In the thermodynamic limit we have as usual

$$\sum_k \equiv \sum_{k^0} \sum_{\mathbf{k}} \to \sum_{k^0}\ V \int \frac{\mathrm{d}^3\mathbf{k}}{(2\pi)^3} \quad (V \to \infty) \ .$$

An explicit calculation of the n–gluon amplitudes in (8–10) is possible if we assume that the average is taken over a Gaussian ensemble, i.e., with an action of the form

$$S[A] \equiv -\frac{1}{2T^2} \sum_{k,k'} A^a_\mu(k)\ (\mathcal{D}^{-1})^{\mu\nu}_{ab}(k,k')\ A^b_\nu(k') \ . \tag{12}$$

Note that $\mathcal{D}$ contains a gauge fixing term. The factor $1/T^2$ is conventional in order that $\mathcal{D}^{\mu\nu}_{ab}$ agrees with the standard definition of the gluon propagator. The assumption of a Gaussian ensemble leads to the factorisation of an arbitrary n–gluon amplitude into a sum over products of all possible pairings of two–gluon amplitudes, i.e., gluon propagators, [30] via

$$\langle A_1 ... A_n \rangle \ = \ \sum_{pairs}\ \langle A_{i_1} A_{i_2} \rangle\ ...\ \langle A_{i_{n-1}} A_{i_n} \rangle \tag{13}$$

$$\langle A^a_\mu(k) A^b_\nu(k') \rangle \ = \ T^2\ \mathcal{D}^{ab}_{\mu\nu}(k,k') \ . \tag{14}$$

In the first line we used a collective index for momentum, Minkowski–, and color–indices. We furthermore assume translation invariance and global color neutrality so that

$$\mathcal{D}^{\mu\nu}_{ab}(k,k') \equiv \mathcal{D}^{\mu\nu}(k)\ \delta_{ab}\ \delta^{(4)}_{k,-k'}\ .$$

With the abbreviation $T/V\sum_k \equiv \int_k$ we obtain

$$\begin{aligned} M^{(0)}(r,0) &= \frac{N_c^2-1}{2}\int_{k,l} e^{-i(k+l)\cdot r}\left[k_x^2\ \mathcal{D}^{yy}(k) - 2\ k_x k_y\ \mathcal{D}^{yx}(k) + k_y^2\ \mathcal{D}^{xx}(k)\right] \\ &\quad \times\left[l_x^2\ \mathcal{D}^{yy}(l) - 2\ l_x l_y\ \mathcal{D}^{yx}(l) + l_y^2\ \mathcal{D}^{xx}(l)\right]\ , \end{aligned} \tag{15}$$

and similar expressions for $M^{(1)}$ and $M^{(2)}$. Each term in eq. (15) has the graphical interpretation shown in Figs. 1a and 1d. We represent the origin O and the point r by "vertices" (without the usual factor g !) and gluon propagators between them by full lines (for free gluons, i.e., $\mathcal{D} \equiv \mathcal{D}_0$ in (15), we use simple full lines as in Fig. 1a, for dressed gluons, we insert a self–energy "bubble" as in Fig. 1d). A cross on the line corresponds to one extra momentum factor or partial derivative. There are three topologically distinct two–loop graphs contributing to $M^{(1)}$ and two three–loop graphs contributing to $M^{(2)}$. Examples of these are illustrated in Figs. 1b and 1c for $\mathcal{D} \equiv \mathcal{D}_0$. However, we do not consider those further, in accordance with our working assumption that the one–loop, two–gluon exchange represents the dominant contribution to the energy density correlators.

Other diagrams which will not be considered in the following arise from non–Gaussian fluctuations, which we have neglected in the factorisation (13), see for instance Fig. 1e. This generic ladder diagram could lead to bound states. In the perturbative picture of the gluon plasma, such a diagram would be suppressed since the ladder interactions are screened by the hot environment. Nevertheless, in view of the analysis of hadronic wavefunctions [16] one cannot a priori rule out that these graphs are not important near T_c. Then, however, the exponential decay of the correlators would be determined by the mass of the exchanged bound gluon pair rather than by twice the screening mass of the two dressed gluons of Fig. 1d. This points to an intrinsic ambiguity in the interpretation of the energy density correlators. Fig. 1f will be discussed in Section 7.

The electric field energy density correlator,

$$E(r,r') \equiv \left\langle \mathrm{Tr}\left[\mathcal{E}_x^2(r) + \mathcal{E}_y^2(r)\right]\ \mathrm{Tr}\left[\mathcal{E}_x^2(r') + \mathcal{E}_y^2(r')\right]\right\rangle_c\ , \tag{16}$$

can be treated in a completely analogous way. As in the magnetic case, our subsequent discussion will be restricted to the one-loop term

$$\begin{aligned} E^{(0)}(r,0) = \frac{N_c^2-1}{2}\int_{k,l} e^{-i(k+l)\cdot r}\sum_{i,j=x,y}&\left[(k^0)^2\mathcal{D}^{ij}(k) - k^0k^j\mathcal{D}^{i0}(k) - k^ik^0\mathcal{D}^{0j}(k) + k^ik^j\mathcal{D}^{00}(k)\right] \\ &\times\left[(l^0)^2\mathcal{D}^{ij}(l) - l^0l^j\mathcal{D}^{i0}(l) - l^il^0\mathcal{D}^{0j}(l) + l^il^j\mathcal{D}^{00}(l)\right]. \end{aligned} \tag{17}$$

We finally project the correlators onto a state with $\omega_n = k_x = k_y = 0$. This is achieved by integrating them over the transverse $\tau - x - y$–plane at r, yielding the *spatial* magnetic

correlator

$$M(z) \equiv \int_0^{1/T} \mathrm{d}\tau \int_{-L/2}^{L/2} \mathrm{d}x \int_{-L/2}^{L/2} \mathrm{d}y \; M(r,0) \; , \tag{18}$$

and similarly for the spatial electric correlator. The integration over the transverse plane eliminates three of the momentum sums in (15) and (17) via the identity

$$\int_0^{1/T} \mathrm{d}\tau \int_{-L/2}^{L/2} \mathrm{d}x \int_{-L/2}^{L/2} \mathrm{d}y \; e^{-ik\cdot r} = e^{ik^z z} \frac{L^2}{T} \; \delta_{k^0,0} \; \delta_{k^x,0} \; \delta_{k^y,0} \; . \tag{19}$$

Explicit expressions will be provided in the next sections when the form of the gluon propagator is specified.

4 The interaction–free case

In this section we discuss the spatial correlators for the case of vanishing coupling $g = 0$ (indicated by subscript 0 at the respective quantities). In this case, the one–loop graph of Fig. 1a is the only term contributing to the correlators and is manifestly gauge invariant. Furthermore, $\mathcal{D}^{\mu\nu}$ in eqs. (15, 17) reduces to the free gluon propagator which in the covariant gauge is given by

$$\mathcal{D}_0^{\mu\nu}(k) = \frac{g^{\mu\nu}}{k^2} - \alpha \; \frac{k^\mu k^\nu}{(k^2)^2} \; . \tag{20}$$

For the integrand in (15) we need the expression

$$k_x^2 \; \mathcal{D}_0^{yy}(k) - 2 \; k_x k_y \; \mathcal{D}_0^{yx}(k) + k_y^2 \; \mathcal{D}_0^{xx}(k) = \frac{k_x^2 + k_y^2}{-k^2} \equiv \frac{k_\perp^2}{\omega_n^2 + k_\perp^2 + k_z^2} \; , \tag{21}$$

where $k_\perp^2 \equiv k_x^2 + k_y^2$. Note that the gauge parameter drops out, as expected. We now insert (15) into (18) and employ (19). Furthermore, in the thermodynamic limit

$$\frac{1}{L} \sum_{k^i} \equiv \int_{-\infty}^{\infty} \frac{\mathrm{d}k^i}{2\pi} \; ,$$

and [31]

$$\int_{-\infty}^{\infty} \frac{\mathrm{d}k^z}{2\pi} \; e^{ik^z z} \; \frac{1}{\tilde{E}^2 + k_z^2} \equiv \frac{1}{2\tilde{E}} \; e^{-\tilde{E}z} \; , \qquad z > 0 \; , \tag{22}$$

where we have introduced the abbreviation $\tilde{E}^2 \equiv \omega_n^2 + k_\perp^2$. We thus arrive at

$$M_0^{(0)}(z) = \frac{N_c^2 - 1}{2} \; T \sum_n \int_0^{\infty} \frac{\mathrm{d}k_\perp k_\perp}{2\pi} \; \frac{k_\perp^4}{4\tilde{E}^2} \; e^{-2\tilde{E}z} \; . \tag{23}$$

We remark that the exponential decay factor in (22) and in the integrand of (23) is generic for spatial correlators. The smallest exponential factor (and thus the dominant term at large distances z) is that for the lowest Matsubara mode and zero transverse momentum.

For further purposes it is convenient to first consider arbitrary (even) powers of transverse momentum in the nominator of the integrand in (23) and to write $\tilde{E}^2 \equiv \mu^2 + k_\perp^2$. In our case, $\mu^2 = \omega_n^2$, but in general, when there is also a mass term in the propagator, $\mu^2 = \omega_n^2 + m^2$. Then, the integral reads

$$\frac{1}{8\pi}\int_0^\infty \mathrm{d}k_\perp k_\perp \, \frac{k_\perp^{2j}}{\mu^2+k_\perp^2} \, e^{-2z\sqrt{\mu^2+k_\perp^2}} \equiv \frac{1}{8\pi} \, \frac{1}{(2z)^{2j}} \, \mathcal{C}_j(2z|\mu|) \; , \tag{24}$$

where the functions

$$\mathcal{C}_j(u) \equiv \int_u^\infty \mathrm{d}y \, \frac{(y^2-u^2)^j}{y} \, e^{-y} \tag{25}$$

are related to the exponential integral. We will only need [32]:

$$\begin{aligned}
\mathcal{C}_0(u) &= -\mathrm{Ei}(-u) \equiv e^{-u}\left(\frac{1}{u} - \mathcal{J}(u)\right) \; , & (26)\\
\mathcal{C}_1(u) &= e^{-u}(1+u) - u^2 \, \mathcal{C}_0(u) \equiv e^{-u}\left(1 + u^2 \mathcal{J}(u)\right) \; , & (27)\\
\mathcal{C}_2(u) &= e^{-u}(6+6u+3u^2+u^3) - 2u^2 \, e^{-u}(1+u) + u^4 \, \mathcal{C}_0(u) \\
&= e^{-u}\left(6+6u+u^2 - u^4 \, \mathcal{J}(u)\right) \; , & (28)
\end{aligned}$$

where

$$\mathcal{J}(u) \equiv \int_0^\infty \mathrm{d}t \; e^{-t} \, \frac{1}{(u+t)^2} \; . \tag{29}$$

Note that

$$\begin{aligned}
\mathcal{C}_j(u) &\sim e^{-u} \; , \quad \text{for } u > 0 \; , & (30)\\
\mathcal{C}_1(0) &= 1 \; , \; \mathcal{C}_2(0) = 6 \; , \quad \text{and} \;\; \mathcal{C}_0(u) \sim \ln u \quad \text{for } u \to 0 \; . & (31)
\end{aligned}$$

In eq. (23), $\mu \equiv \omega_n$, and thus

$$\begin{aligned}
\frac{M_0^{(0)}}{T^5}(zT) &= \frac{N_c^2-1}{16\pi} \, \frac{1}{(2zT)^4} \sum_{n=-\infty}^{\infty} \mathcal{C}_2(2z|\omega_n|) \\
&= \frac{N_c^2-1}{16\pi} \, \frac{1}{(2zT)^4} \left\{ \mathcal{C}_2(0) + 2\sum_{n=1}^{\infty} \mathcal{C}_2(4\pi n z T) \right\} \; . & (32)
\end{aligned}$$

With eq. (28), the sum over n can be further simplified using identities for the geometrical progression and its derivatives. For the following discussion, however, the form (32) is more convenient.

Let us first estimate the behavior of the correlator for different regions of zT. For very small distances $zT \ll 1$, one expects that temperature effects do not play a role and that the behavior of the correlator is solely determined by dimensional arguments, as it would also be the case at $T = 0$. Since $M(r,0) \sim r^{-8}$, we conclude that due to the integration over the $\tau - x - y$–plane in (18) $M(z)$ must be $\sim z^{-5}$ [18]. Indeed, taking that term in (28), which is dominant for small zT, and employing the geometrical progression one easily shows that

the sum over Matsubara frequencies $n \neq 0$ in (32) diverges as $1/zT$, and hence $M_0^{(0)}/T^5$ has the expected $(zT)^{-5}$–singularity.

At larger zT the contributions of the non–zero Matsubara modes decay exponentially according to (30). Therefore, by virtue of (31), the first term in curly brackets (corresponding to $n = 0$) is the dominant term for large zT. This changes the small distance $(zT)^{-5}$–behavior to a decay proportional to $(zT)^{-4}$. Thus, finite temperature enhances long distance correlations by one power of the distance as compared to the $T = 0$–case (in our case, from z^{-5} to z^{-4}). This is a generic feature for *all* correlation functions at finite temperature and is essentially caused by the replacement of the time integration by T times a Matsubara sum in finite–temperature field theory [33].

These expectations are confirmed in Fig. 2a where we have plotted the full result (32) and the contribution of the zero mode as a function of zT. For small zT, the non–zero Matsubara modes ($\sim (zT)^{-5}$ for $zT \to 0$) dominate over the $n = 0$–term (dotted line) which is only $\sim (zT)^{-4}$, but already for $zT \approx 1/2$, they become negligibly small due to the exponential suppression, and the decay of the correlator is $\sim (zT)^{-4}$.

Note that since $\mathcal{C}_2(0)$ is *constant*, cf. eq. (31), the decay of the spatial correlator in the interaction–free case is *polynomial*, $\sim (zT)^{-4}$ for $zT \geq 1/2$. However, as will be discussed in the next section, in the case of screening interactions the gluon will acquire a mass m. As mentioned above, this has the effect that $\mu = \omega_n \to (\omega_n^2 + m^2)^{1/2}$, and the $n = 0$–term in (32) becomes $\mathcal{C}_2(2zm)$. Consequently, it *also decays exponentially* on account of (30). This exponential decay is superimposed on the polynomial $(zT)^{-4}$–decay and of course dominates for large zT. At distances where zT as well as zm are small, however, the scales set by the temperature or the mass, respectively, cannot play a role and the correlator must again exhibit a z^{-5}–singularity as expected from dimensional arguments.

Employing eq. (17), the analogue of (18) for the electric case, and eqs. (20, 22), the electric correlator reads

$$E_0^{(0)}(z) = \frac{N_c^2 - 1}{2}\, T \sum_n \int_0^\infty \frac{\mathrm{d}k_\perp k_\perp}{2\pi}\, \frac{k_\perp^4 + 2\,\omega_n^2 \tilde{E}^2}{4\tilde{E}^2}\, e^{-2\tilde{E}z}\ , \tag{33}$$

and can therefore be partly expressed in terms of the magnetic correlator,

$$\begin{aligned} \frac{E_0^{(0)}}{T^5}(zT) \;&\equiv\; \frac{M_0^{(0)}}{T^5}(zT) \\ &+\; \frac{N_c^2 - 1}{4\pi}\, \frac{1}{(2zT)^4} \sum_{n=1}^{\infty} (4\pi n z T)^2 \Big\{ \mathcal{C}_1(4\pi n z T) + (4\pi n z T)^2\, \mathcal{C}_0(4\pi n z T) \Big\}\ . \end{aligned} \tag{34}$$

Again, the sum can be analytically performed using identities for the geometrical progression.

In Fig. 2b we show the electric correlator in comparison to the magnetic correlator. As expected from (30), the additional terms in the electric correlator (34) are negligible for $zT \geq 1$ and only influence the domain of $0.1 \leq zT \leq 1$. For very small $zT \leq 0.1$, however, the electric correlator becomes equal to the magnetic (and thus has the same dominant singularity $\sim (zT)^{-5}$). The reason is that electric and magnetic fields are indistinguishable in Euclidean field theory at $T = 0$ or at distances where the scale set by the temperature becomes irrelevant, respectively.

5 Correlators in the case of dressed propagators

In this section we study the effect of the hot environment on the one–loop energy density correlators. To this end we assume that the two gluon propagators connecting O and r acquire a self–energy modification, see Fig. 1d. The "dressed" propagator reads (in covariant gauge) [6]

$$\mathcal{D}^{\mu\nu}(k) = \frac{\mathcal{P}^{\mu\nu}}{k^2 - \pi_T} + \frac{\mathcal{Q}^{\mu\nu}}{k^2 - \pi_L} + (1-\alpha)\,\frac{k^\mu k^\nu}{(k^2)^2}\;, \tag{35}$$

with the two–space projectors

$$\mathcal{P}^{\mu\nu} \;\equiv\; \Delta^{\mu\nu} + \frac{\tilde{k}^\mu \tilde{k}^\nu}{\mathbf{k}^2}\;, \tag{36}$$

$$\mathcal{Q}^{\mu\nu} \;\equiv\; g^{\mu\nu} - \frac{k^\mu k^\nu}{k^2} - \mathcal{P}^{\mu\nu}\;, \tag{37}$$

where $\Delta^{\mu\nu} \equiv g^{\mu\nu} - u^\mu u^\nu$, $\tilde{k}^\mu \equiv \Delta^{\mu\nu} k_\nu$. u^μ is the (collective) 4–velocity of the matter under consideration.

We now consider the combination of k^i and $\mathcal{D}^{ij}$ appearing in eq. (15) in the rest frame of matter, $u^\mu = (1,0,0,0)$. We find the simple gauge invariant result

$$k_x^2\;\mathcal{D}^{yy}(k) - 2\;k_x k_y\;\mathcal{D}^{yx}(k) + k_y^2\;\mathcal{D}^{xx}(k) = \frac{k_x^2 + k_y^2}{-k^2 + \pi_T} = \frac{k_\perp^2}{\omega_n^2 + k_\perp^2 + k_z^2 + \pi_T}\;, \tag{38}$$

which should be compared with (21). The only modification thus far is the appearance of the "gluon mass" $\sqrt{\pi_T}$. In the general case, π_T depends non–trivially on k^μ. This may be seen considering for instance the gauge–invariant part of the one–loop gluon self–energy [6, 34]. Only for $k^\mu = (0,\mathbf{k})$, i.e., for the lowest Matsubara frequency, the dependence is trivial: $\pi_T(0,\mathbf{k}) \equiv 0$ for all $\mathbf{k}$, indicating the absence of screening of static magnetic fields in first order perturbation theory. Static magnetic fields are screened in higher order in g, but this is not perturbatively calculable. On the other hand, lattice calculations may provide this information. As mentioned in Section 2, the results of [1] were interpreted exactly in the way that they represent a non–perturbative measurement of the magnetic screening mass $m_M \equiv (\lim_{\mathbf{k}\to 0}\pi_T(0,\mathbf{k}))^{1/2}$.

Given $\pi_T(k)$, in the general case one would have to perform the Fourier–transformation (22), with $\tilde{E}$ replaced by

$$\tilde{E}_T \equiv \sqrt{\omega_n^2 + k_\perp^2 + \pi_T}\;, \tag{39}$$

and the subsequent integration over transverse momenta, cf. eq. (23), numerically. However, since there is up to now no way to obtain an analytical expression for π_T, we may as well make the simplifying assumption that $\pi_T \equiv const.$, in order to proceed analytically. In this case, we anticipate (see also the discussion in the previous section) that the only modification of the final result in comparison to the interaction–free case will be an exponential damping of the correlator due to the gluon mass $\sqrt{\pi_T}$.

Indeed, for constant π_T, the result (22) for the Fourier–transformation still applies (with $\tilde{E}$ replaced by $\tilde{E}_T$) and we are left with the integral over transverse momenta, which is – after our groundwork in the previous section – readily expressed in terms of $\mathcal{C}_2$:

$$\frac{M^{(0)}}{T^5}(zT) = \frac{N_c^2-1}{16\pi}\,\frac{1}{(2zT)^4}\left\{\,\mathcal{C}_2(2z\sqrt{\pi_T}) + 2\sum_{n=1}^{\infty}\,\mathcal{C}_2(2z\Omega_n^T)\right\}\,, \tag{40}$$

where $\Omega_n^T \equiv (\omega_n^2+\pi_T)^{1/2}$. On dimensional grounds $\pi_T = CT^2$, where C is dimensionless. In the absence of any other scale C is independent of T, and thus the right–hand side of (40) is still a function of zT only (as indicated in the argument on the left–hand side).

For the following, we may assume $C \sim 1$. Then, for finite n we have $4\pi^2n^2T^2 \approx 40\,n^2T^2 \gg \pi_T \sim T^2$, and consequently $\Omega_n^T \approx 2\pi nT$. Thus, as required from dimensional arguments, we recover the $(zT)^{-5}$–singularity for $zT \to 0$, i.e., on scales where neither the temperature nor the gluon mass $\sqrt{\pi_T}$ (which is assumed to be of the order of T anyway) are relevant. In addition, the exponential decay of the $n \neq 0$–terms for large zT is similar to the interaction–free case. Consequently, these terms can be neglected for $zT \geq 1/2$. The most important modification as compared to (32) occurs for $n = 0$. In the interaction–free case, we had $\mathcal{C}_2(0) = 6$, cf. (31), leading to a *purely polynomial decay* $\sim (zT)^{-4}$ of the correlator (32) for large zT. Now, however, due to the appearance of the gluon mass $\sqrt{\pi_T}$, $\mathcal{C}_2(2z\sqrt{\pi_T}) \sim \exp\{-2z\sqrt{\pi_T}\}$ according to (30), i.e., *an exponential decay* is superimposed onto the polynomial decay and, of course, *dominates at large* zT. The corresponding slope is given by $2\sqrt{\pi_T}$, i.e., since $m_M \equiv \sqrt{\pi_T}$, by twice the magnetic gluon screening mass, as argued in Section 2. However, we expect that in the region of small zT the $(zT)^{-4}$–behavior and the $(zT)^{-5}$–singularity still influence the correlator to a large extent.

For the electric correlator the combination of k^μ and $\mathcal{D}^{\mu\nu}$ occurring in eq. (17) reads with (35)

$$\begin{aligned}
&(k^0)^2\mathcal{D}^{ij}(k) - k^0k^j\mathcal{D}^{i0}(k) - k^ik^0\mathcal{D}^{0j}(k) + k^ik^j\mathcal{D}^{00}(k)\\
&= \frac{\delta^{ij}-k^ik^j/\mathbf{k}^2}{-k^2+\pi_T}\,k_0^2 - \frac{-k^2}{-k^2+\pi_L}\,\frac{k^ik^j}{\mathbf{k}^2}\\
&= \frac{-\omega_n^2}{\tilde{E}_T^2+k_z^2}\,\delta^{ij} - k^ik^j\,\left\{\frac{1}{\tilde{E}_L^2+k_z^2} - \frac{\omega_n^2}{k_\perp^2+k_z^2}\left(\frac{1}{\tilde{E}_T^2+k_z^2} - \frac{1}{\tilde{E}_L^2+k_z^2}\right)\right\}\,,
\end{aligned} \tag{41}$$

where we have defined $\tilde{E}_L^2 = \omega_n^2 + k_\perp^2 + \pi_L$ in analogy to (39). Again, this result is gauge invariant.

It is noteworthy that not only π_L enters the expression for the electric correlator, but also π_T. The reason is that there is a transverse gluon $\mathcal{A}^i$ involved in the definition of $E(r,0)$. One might therefore suspect that the exponential decay of the electric correlator will be eventually dominated by the smaller polarization function which could be π_T, at least at high temperatures where $g \ll 1$ and $\pi_T \sim g^4T^2 \ll \pi_L \sim g^2T^2$. Nevertheless, this is not the case: in eq. (41) the respective terms are always accompanied by a factor of ω_n^2, thus they only contribute for non–zero Matsubara frequencies. As we have seen, these terms are in general strongly suppressed for large z. Furthermore, note that due to the structure of the projectors $\mathcal{P}^{\mu\nu}$ and $\mathcal{Q}^{\mu\nu}$, there is also a denominator $k_\perp^2 + k_z^2$.

The electric correlator is given by inserting (41) into (17). Again, further progress is possible under the assumption that both π_T and π_L are constant. As mentioned above, to one–loop order this is only true for $k^\mu = (0, \mathbf{k})$: $\pi_T(0,\mathbf{k}) \equiv 0$ and $\pi_L(0,\mathbf{k}) \equiv m_E^2$. The Fourier–transformation can be performed using (22) and [35]

$$\int_{-\infty}^{\infty} \frac{\mathrm{d}x}{2\pi}\, e^{ixz}\, \frac{1}{(a^2+x^2)(b^2+x^2)} = \frac{a\, e^{-bz} - b\, e^{-az}}{2ab\, (a^2-b^2)}\ , \quad a,b,z>0\ .$$

We rearrange the final result in terms proportional to the various exponential decay factors,

$$\begin{aligned} E^{(0)}(z) = \frac{N_c^2-1}{16\pi}\, T \sum_{n=-\infty}^{\infty} \int_0^\infty \mathrm{d}k_\perp k_\perp \Bigg\{ \omega_n^4 \Bigg(\left[\frac{1}{\tilde{E}_T^2} + \frac{\tilde{E}_T^2}{(\Omega_n^T)^4}\right] e^{-2\tilde{E}_T z} \\ + \frac{\pi_T-\pi_L}{(\Omega_n^T\Omega_n^L)^2}\, \frac{2k_\perp}{\tilde{E}_T} \left[1+\frac{k_\perp^2}{(\Omega_n^T)^2}\right] e^{-(k_\perp+\tilde{E}_T)z} + \frac{(\pi_T-\pi_L)^2}{(\Omega_n^T\Omega_n^L)^4}\, k_\perp^2\, e^{-2k_\perp z}\Bigg) \\ + \omega_n^2\, \frac{\pi_L}{(\Omega_n^T\Omega_n^L)^2}\, \frac{2k_\perp^2}{\tilde{E}_L} \left(\frac{\pi_T-\pi_L}{(\Omega_n^L)^2}\, k_\perp\, e^{-(k_\perp+\tilde{E}_L)z} + \tilde{E}_T\, e^{-(\tilde{E}_T+\tilde{E}_L)z}\right) + \frac{\pi_L^2}{(\Omega_n^L)^4}\, \frac{k_\perp^4}{\tilde{E}_L^2}\, e^{-2\tilde{E}_L z}\Bigg\}\ . \end{aligned} \tag{42}$$

Here we have also introduced $\Omega_n^L \equiv (\omega_n^2+\pi_L)^{1/2}$. The integration over transverse momenta can be done analytically, but the result is extremely unwieldy. In fact, most of the terms are rapidly suppressed for increasing z, since they are accompanied by terms $\sim \omega_n^2\, \exp\{-z\Omega_n^{T,L}\}$. As we will see, for a qualitative discussion of the correlator it is sufficient to retain only the last terms in the second and the third line of eq. (42),

$$\int_0^\infty \mathrm{d}k_\perp k_\perp\, k_\perp^2\, e^{-2k_\perp z} = \frac{1}{(2z)^4}\, \mathcal{C}_2(0)\ , \tag{43}$$

$$\int_0^\infty \mathrm{d}k_\perp k_\perp\, \frac{k_\perp^4}{\tilde{E}_L^2}\, e^{-2\tilde{E}_L z} = \frac{1}{(2z)^4}\, \mathcal{C}_2(2z\Omega_n^L)\ . \tag{44}$$

For small z, the Matsubara sum over the terms (44) provides the z^{-5}–singularity expected from dimensional arguments. For $zT \geq 1$ and finite n, the term (44) becomes irrelevant, because it is exponentially suppressed $\sim \exp\{-2z\Omega_n^L\} \approx \exp\{-4\pi n z T\}$ on account of (30). For $n=0$, however, (a) it is the only term in (42) which does not vanish and (b) it exhibits the weakest *exponential* decay $\sim \exp\{-2z\sqrt{\pi_L}\}$ of all terms in (42). The slope of this decay is twice the electric screening mass $m_E \equiv \sqrt{\pi_L}$. The term (43) is only *polynomially* decaying ($\sim z^{-4}$) since $\mathcal{C}_2(0)=6$, and will thus eventually dominate the long–distance behavior of the correlator (42), provided $\pi_T \neq \pi_L$ (which appears as a prefactor to (43) in (42)). Note that this term arises from the Fourier–transformation of the denominator $k_\perp^2 + k_z^2$ in (41) which in turn originates from the specific structure of the projectors in eq. (35). For $zT \geq 1$ the approximate form of the electric correlator is

$$\frac{E^{(0)}}{T^5}(zT) \approx \frac{N_c^2-1}{16\pi}\, \frac{1}{(2zT)^4} \left\{ \mathcal{C}_2(2z\sqrt{\pi_L}) + 12\, (\pi_T-\pi_L)^2 \sum_{n=1}^{\infty}\, \frac{\omega_n^4}{(\Omega_n^T\Omega_n^L)^4}\right\}\ . \tag{45}$$

In Fig. 3a we show the electric and magnetic correlator, normalized to T^5, as a function of zT for $\pi_L = (1.4\,T)^2$, $\pi_T = (2.9\,T)^2$ in comparison to the free case. This choice for the

polarization functions is motivated by the results of Ref. [1], where it was found that the electric correlator decays with the rate $2\,m_E \equiv 2\sqrt{\pi_L} \approx 2.8\,T$ and the magnetic correlator with the rate $2\,m_M \equiv 2\sqrt{\pi_T} \approx 5.8\,T$.

One observes that the power–law behavior found in the interaction–free case dominates both correlators up to $zT \approx 2$. For larger zT the exponential decay prevails for the magnetic while for the electric correlator an anomalous power–law decay is observed due to the second term in (45). This is shown in detail in Fig. 3b, where the various contributions to the electric correlator are plotted separately. The precise value of zT at which the power–law term dominates over the exponentially decaying first term in (45) depends on π_T and π_L. This anomaly is an artefact from our simplifying assumption that the polarization functions do not vanish for large $\mathbf{k}$ and non–zero ω_n. In general we expect that for large zT the electric correlator decays exponentially on the scale $2\,m_E$.

6 Lattice correlators in the weak–coupling limit

Due to the periodicity of the lattice, a simulation can follow the decay of any correlator only up to $z/L = 1/2$, where $L = aN_\sigma$ is the spatial extension of the lattice. This point corresponds, for any lattice with $N_\sigma = 4\,N_\tau$, to $zT = 2$. What is surprising is that in the lattice simulations of [1] there is no hint of the power–law behavior which we have found to dominate the correlators for $zT \leq 2$ in our above continuum analysis. As we will show in the next section, this could be due to the use of fuzzed links [36].

In this section we quantify effects arising from the discretization and the finite lattice size without distortion from additional signal enhancement prescriptions. For this purpose it is sufficient to only consider the magnetic correlator. The transcription of eq. (15) onto a finite lattice proceeds along the lines given in [37]. After switching to the Euclidean metric, the main difference between the continuum and the lattice formulation is (a) that the gluon fields live in the middle of a link

$$A^b_\mu(x) = \frac{1}{N_\sigma^3 N_\tau a^4} \sum_k e^{ik_\alpha(x+a\mathbf{e}_\mu/2)_\alpha}\; A^b_\mu(k)\;, \tag{46}$$

where $\mathbf{e}_\mu$ is the lattice unit vector pointing in μ–direction, and (b) that partial derivatives are replaced by forward finite differences,

$$\partial_\nu A^b_\mu(x) \;\rightarrow\; \frac{A^b_\mu(x+a\mathbf{e}_\nu) - A^b_\mu(x)}{a}\;. \tag{47}$$

The momenta in (46) fulfill

$$\begin{aligned} k_i &= \frac{2\pi j_i}{aN_\sigma}\;,\quad j_i = 0,...,N_\sigma - 1\;,\quad i = x,y,z\;, \\ k_0 &= \frac{2\pi j_0}{aN_\tau}\;,\quad j_0 = 0,...,N_\tau - 1\;. \end{aligned}$$

The free lattice action closely resembles the continuum action (12),

$$S_0[A] = -\frac{1}{2N_\sigma^3 N_\tau a^4} \sum_k A_\mu^b(-k)\ \mathcal{D}^{-1}_{0,\mu\nu}(k)\ A_\nu^b(k)\ , \tag{48}$$

with

$$\mathcal{D}^{-1}_{0,\mu\nu}(k) = \delta_{\mu\nu}\ \left(m^2 + \frac{4}{a^2} \sum_{\rho=\tau}^{z} \sin^2\left[\frac{k_\rho a}{2}\right]\right)\ , \tag{49}$$

where we have introduced a mass term. On the one hand, this allows to regularize any singularities due to constant field configurations. Usually, these singularities are avoided by omitting the $k_0 = k_x = k_y = k_z$–term in momentum sums [37]. We will see that this is not necessary here: even for $m = 0$ such a term is finite in the correlator (see below). On the other hand, allowing for a finite m from the outset provides a simple way to include a screening mass in the final expression. In the following, we will also make use of the relation

$$\left\langle A_\mu^b(k)\ A_\nu^c(l)\right\rangle_0 = \delta_{bc}\ \delta^{(4)}_{k,-l}\ N_\sigma^3 N_\tau a^4\ \mathcal{D}_{0,\mu\nu}(k)\ . \tag{50}$$

Given these facts, it is straightforward to derive the magnetic correlator

$$M_0^{(0)}(r,0) \equiv \left\langle \mathrm{Tr}\ \mathcal{F}_{xy}^2(r)\ \mathrm{Tr}\ \mathcal{F}_{xy}^2(0)\right\rangle_{0,c} = \frac{N_c^2-1}{2}\left(\ \frac{1}{N_\sigma^3 N_\tau a^4}\ \frac{4}{a^2}\ \sum_k\ e^{ik\cdot r}\right. \tag{51}$$

$$\left.\times\quad \left\{\sin^2\left[\frac{k_x a}{2}\right]\ \mathcal{D}_{0,yy}(k) - 2\sin\left[\frac{k_x a}{2}\right]\sin\left[\frac{k_y a}{2}\right]\ \mathcal{D}_{0,xy}(k) + \sin^2\left[\frac{k_y a}{2}\right]\ \mathcal{D}_{0,xx}(k)\right\}\right)^2\ .$$

The main difference as compared to (15) is that k^i is replaced by $2\sin[k_i a/2]$, as usual for bosons on the lattice. Summing over the $\tau-, x-$, and $y-$sites at constant z in order to project onto zero momentum and employing (49) we obtain

$$M_0^{(0)}(z)(aN_\tau)^5 = \frac{N_c^2-1}{2}\ \frac{N_\tau^4}{N_\sigma^2} \sum_{k_0,k_x,k_y} \left(\frac{4}{N_\sigma}\ \sum_{k_z}\ e^{ik_z z}\ \frac{\sin^2[k_x a/2] + \sin^2[k_y a/2]}{(ma)^2 + 4\sum_\rho \sin^2[k_\rho a/2]}\right)^2\ . \tag{52}$$

The Fourier–transformation can be done using the identity

$$\frac{1}{N_\sigma} \sum_{j_z=0}^{N_\sigma-1} \frac{\cos[2\pi j_z z/aN_\sigma]}{\omega^2 + \sin^2[\pi j_z/aN_\sigma]} \equiv 2\ \frac{\cosh\left[2\hat\omega(N_\sigma/2 - z/a)\right]}{\sinh[2\hat\omega]\ \sinh[N_\sigma\hat\omega]}\ , \tag{53}$$

which can be proven by contour integration. Here $\hat\omega = \ln[\omega + \sqrt{\omega^2+1}]$ and

$$\omega^2 \equiv \left(\frac{ma}{2}\right)^2 + \sum_{\rho=\tau,x,y} \sin^2\left[\frac{k_\rho a}{2}\right]\ .$$

The reason why there is no singularity in (52) in the case $m = 0$ due to constant field configurations ($k_0 = k_x = k_y = k_z = 0$) is that the term $\sin^2[k_x a/2] + \sin^2[k_y a/2]$ regulates this singularity. Nevertheless, the limit $m \to 0$ is subtle: putting $m = 0$ *from the outset*,

the zero momentum term is *finite*, while performing the limit $m \to 0$ *after* calculating the correlator, this term *vanishes*. Since the theory is not well-defined in the first case, we will always use the second prescription when considering the case $m = 0$ in the following.

In the case of a dressed gluon propagator one would in principle have to use the lattice analogues for the decomposition (35) and for the polarization functions $\pi_{T,L}$ [38]. However, for an estimate of lattice effects and the general behavior of the correlator on the lattice it is certainly sufficient to simply assume a finite constant mass $m \equiv \sqrt{\pi_T}$ in the above expression (52). This assumption is supported by a comparison of (51) and the continuum analogue (15) with (38).

The resulting correlator is shown in Fig. 4a for $\pi_T = 0$ and $\pi_T = (2.9\,T)^2$ in comparison to the corresponding continuum expression. One observes that the lattice ultraviolett cut–off a^{-1} regulates the z^{-5}–singularity at the origin, but that otherwise, on the 4×16^3–lattice used in [1], the continuum limit is quite well reproduced. This, however, implies that the power–law behavior still influences the decay of the correlator. This has important consequences for the extraction of a screening mass. A fit with a simple exponential $\exp\{-\mu(z)z\}$, or, on a finite lattice with a hyperbolic cosine $\cosh[\mu(z)(aN_\sigma/2 - z)]$ [1] (due to the lattice symmetry centered at $z/L = 1/2$), will necessarily lead to local masses $\mu(z)$ which are *larger* than $2\sqrt{\pi_T}$ (or $2\sqrt{\pi_L}$ in the electric case). Thus, screening masses extracted from these local masses via the simple relation $\mu(z) = 2\,m_{E,M}$ *overestimate* the actual values.

To quantify this we extract local masses from the correlators via

$$\frac{M_0^{(0)}(z)}{M_0^{(0)}(z-a)} = \frac{\cosh[\mu(z)(aN_\sigma/2 - z)]}{\cosh[\mu(z)(aN_\sigma/2 - (z-a))]}\,, \tag{54}$$

which is the same procedure as used in Ref. [1]. If this prescription worked correctly, the local mass should be two times the gluon mass, i.e., $\mu(z)a \equiv 2\,ma = 2\sqrt{\pi_T/T^2}/N_\tau = 1.45 = \mu_{real}a$ ($N_\tau = 4$ and $\pi_T = (2.9\,T)^2$). However, as one observes in the first row of Table 1 (see also Fig. 5a), even at $z/a = 6$ the local mass overestimates the actual value by 35% !

However, our results are not yet directly comparable to that of [1]. First of all, in that work sources and sinks of the correlators are plaquettes with a minimum edge length a, while (52) is essentially a point–to–point correlator. In addition, *fuzzed links* were used to enhance the signal at large z [19]. This technique effectively enlargens sources and sinks to the size of several plaquettes and also suppresses contributions of higher excited states at small z [39], thus having an effect similar to wall sources commonly employed in the calculation of hadronic correlation functions. In the next section we investigate a model for fuzzing and apply it to our perturbative correlators.

To conclude this section we remark that excited states are in our picture essentially states of *non–zero* transverse momentum and Matsubara frequency in the gluon loop in Figs. 1a,d. The summation over these excited states is nothing but the integration over transverse momenta and summation over Matsubara frequencies in (23) or (42). In this sense, the common notion that higher excited states enhance the point–to–point correlator at small distances is just reflected by our observation that the integration over transverse momenta and the summation over Matsubara frequencies leads to polynomial enhancement for small z.

Table 1

z/a	1	2	3	4	5	6	$\mu_{real}a$	L_τ	L_σ
$\mu(z)a$	4.09	3.58	2.95	2.45	2.15	1.95	1.45	0	0
	3.28	2.86	2.50	2.24	2.06	1.91	1.45	1	1
	2.91	2.50	2.25	2.08	1.97	1.85	1.45	2	2
	2.80	2.29	2.01	1.89	1.81	1.72	1.45	2	4
	2.79	2.25	1.92	1.77	1.70	1.62	1.45	2	8
$\mu(z)a$	3.83	2.93	1.87	1.26	0.96	0.77	0	0	0
	2.83	2.11	1.52	1.16	0.93	0.76	0	1	1
	2.30	1.69	1.31	1.07	0.89	0.74	0	2	2
	1.97	1.31	1.05	0.92	0.81	0.71	0	2	4
	1.80	1.10	0.89	0.81	0.74	0.66	0	2	8

7 Extended correlators

Fuzzed links are obtained by replacing each link by a sum of products of two or more links in the vicinity of the old link [19]. This roughly doubles the size of plaquettes at each new level of fuzzing and thus smears out the sources and sinks of the plaquette correlators.

In our continuum analysis, we model fuzzing by introducing form factors, $\Phi(\Delta r)$ and $\Phi'(\Delta r')$, for the smeared sink and source, respectively, and study the extended correlator

$$\mathcal{M}(z) \equiv \frac{T}{L^2}\int \mathrm{d}^3r_1\ \mathrm{d}^3r_2\ \mathrm{d}^3r_1'\ \mathrm{d}^3r_2'\ \Phi(\Delta r)\ \Phi'(\Delta r')\ \mathcal{M}(r_1,r_2,r_1',r_2')\ , \quad (55)$$

$$\mathcal{M}(r_1,r_2,r_1',r_2') \equiv \langle \mathrm{Tr}[\mathcal{B}_z(r_1)\mathcal{B}_z(r_2)]\ \mathrm{Tr}[\mathcal{B}_z(r_1')\mathcal{B}_z(r_2')]\rangle_c\ , \quad (56)$$

where $\Delta r \equiv r_1 - r_2$, $\Delta r' \equiv r_1' - r_2'$ ($\Delta z = \Delta z' = 0$) and $\mathrm{d}^3r_i \equiv \mathrm{d}\tau_i\,\mathrm{d}x_i\,\mathrm{d}y_i$, $i = 1,2$, and similarly for d^3r_i'. Note that, analogous to fuzzing [1, 19], smearing is limited to the transverse and temporal directions with $z_1' = z_2' = 0$ and $z_1 = z_2 = z$ held fixed. Equation (55) reduces to (18) for the choice $\Phi(\Delta r) = \delta^{(3)}(\Delta r)$, $\Phi'(\Delta r') = \delta^{(3)}(\Delta r')$. The prescription (55) is chosen such that (a) the only modification of the one–loop contribution (23) is the additonal appearance of the Fourier–transformed form factors $\tilde{\Phi}(-\omega_n, -\mathbf{k}_\perp)$ and $\tilde{\Phi}'(\omega_n, \mathbf{k}_\perp)$ and (b) its gauge invariance is preserved due to (21).

It is obvious that with suitable form factors one can suppress the contribution of large $k_\perp$ and n. Thus, our model correctly simulates the effect of fuzzing in that the small–z enhancement of the correlation function due to higher excited states can be reduced, which leaves the exponential decay less distorted. Diagramatically, the above prescription replaces Fig. 1d with point source and sink with Fig. 1f, where the two dressed gluons are produced and absorbed from an extended source and sink, respectively.

For example, *wall sources* correspond to the special choice $\Phi'(\Delta r') = T/L^2 \equiv const.$, $\Phi(\Delta r) = \delta^{(3)}(\Delta r)$. This corresponds to $\tilde{\Phi}'(\omega_n, \mathbf{k}_\perp) = \delta_{n,0}\ \delta^{(2)}_{\mathbf{k}_\perp,0}$, $\tilde{\Phi} = 1$, which has the maximum effect of suppressing *all* higher transverse momenta and Matsubara frequencies. Unfortunately, wall sources are not applicable in our case, since the contribution of zero

transverse momentum has zero measure in the integral in (23) and would thus lead to a trivial result for the correlator.

We now investigate the influence of smeared sources and sinks on the lattice correlator (52). To this end, eq. (55) is transcribed onto the lattice using standard discretization prescriptions. In [1] the sources and sinks prior to fuzzing are plaquettes of edge length a. Fuzzing links up to fuzzing level l increases the *average* edge length of the plaquette source and sink to $2^l a$ [19]. Consequently, the sources and sinks have on the average the volume $L_\tau a \times (L_\sigma a)^2$ where $L_\tau \equiv 2^{l_\tau}$, $L_\sigma \equiv 2^{l_\sigma}$. Thus, we choose as form factor

$$\Phi(r) \equiv \frac{1}{a^3(L_\tau+1)(L_\sigma+1)^2} \sum_{n_\tau=0}^{L_\tau} \sum_{n_x,n_y=0}^{L_\sigma} \delta_{\tau,n_\tau a}\, \delta_{x,n_x a}\, \delta_{y,n_y a}\ , \tag{57}$$

and the same for Φ'. This corresponds to a homogeneous smearing of the source and sink over a cube of volume $L_\tau a \times (L_\sigma a)^2$. Clearly many other possibilities for form factors are possible, but (57) is the most simple choice and will be adequate to prove our point, namely, that the extracted screening masses are extremely sensitive to the chosen smearing prescription and that smearing improves the extraction of screening masses only in the case when those are large compared to T. For small screening masses smearing will be seen to introduce uncontrolled errors.

The fuzzing level used in [1] is $l_{\tau,\sigma} = \log_2 N_{\tau,\sigma} - 1$, i.e., $l_\sigma = 3$ and $l_\tau = 1$ for the 4×16^3–lattice under consideration. Consequently, $L_\sigma = 8$ and $L_\tau = 2$. However, in order to study systematically the influence of our "fuzzing" prescription, we vary L_σ from 0 to 8 and L_τ from 0 to 2 (see Table 1 and Figs. 4b,c, and 5a). Note that since sources and sinks of the correlators studied in [1] are elementary plaquettes of edge length a prior to fuzzing, for instance an "unfuzzed" P_s–correlator should actually not be compared to our magnetic point–to–point correlator of Section 6, but rather to an extended correlator with $L_\tau = 0$, $L_\sigma = 1$. The Fourier–transform of (57) is

$$\begin{aligned} \tilde{\Phi}(\omega_n, \mathbf{k}_\perp) &= a^3 \sum_{\tau,x,y} e^{-i(\omega_n \tau + k_x x + k_y y)}\, \Phi(r) \\ &= \frac{1}{(L_\tau+1)(L_\sigma+1)^2} \sum_{n_\tau=0}^{L_\tau} \sum_{n_x,n_y=0}^{L_\sigma} e^{-ia(\omega_n n_\tau + k_x n_x + k_y n_y)}\ . \end{aligned} \tag{58}$$

The result (52) is modified in that the modulus squared of (58) appears additionally under the sum over k_0, k_x, k_y. Using [40], one obtains the simple analytical expression

$$|\tilde{\Phi}(\omega_n, \mathbf{k}_\perp)|^2 = \left(\frac{\sin[a\omega_n(L_\tau+1)/2]}{(L_\tau+1)\sin[a\omega_n/2]} \, \frac{\sin[ak_x(L_\sigma+1)/2]}{(L_\sigma+1)\sin[ak_x/2]} \, \frac{\sin[ak_y(L_\sigma+1)/2]}{(L_\sigma+1)\sin[ak_y/2]} \right)^2 . \tag{59}$$

The correlator is displayed in Fig. 4b for $\pi_T = (2.9\,T)^2$ and in Fig. 4c for $\pi_T = 0$ for different degrees of smearing. One clearly observes a suppression of the polynomial enhancement at small z, which is proportional to the degree of smearing of sources and sinks. This reflects the sensitivity of the correlators and hence the extracted screening masses to the choice of the form factor and thus to the particular fuzzing prescription. In the case of maximal smearing

$L_\sigma = 8$, $L_\tau = 2$ the decay of the correlator for $\pi_T = (2.9\,T)^2$ is very close to exponential, which is confirmed by the fact that the local masses are nearly constant for $2 \leq z/a \leq 6$. This can be seen from Table 1 and Fig. 5a. However, while the reduction of the error due to smearing is impressive for small z, the overestimate is still approximately 12% at $z/a = 6$.

Reversing this argument, one could ask for the value of the *real* screening mass that would lead to an observed *local* mass near the value $\mu(z)a \approx 1.45$. To this end, consider first the local masses extracted from the *free* correlator (Fig. 4c). One observes (cf. Table 1 and Fig. 5a) that the sensitivity of the local masses to the degree of smearing (and thus the fuzzing prescription) is even more pronounced than in the finite mass case, especially for small z. However, the striking feature is that, although the *theoretically assumed screening mass is zero*, the *local mass* extracted via the exponential–type fit (54) is *finite* ! This is independent of the degree of smearing, although more strongly smeared sources and sinks give smaller values for the local mass. Nevertheless, the local mass extracted via (54) fails completely to approximate the real mass if the latter is small compared to T.

To compare with the results of [1] we have to bear in mind that our perturbative analysis relies on the assumptions that (a) plaquette correlators can be approximated by energy density correlators, (b) the main contribution to the energy density correlators is the exchange diagram of Fig. 1d, and (c) that our smearing prescription accurately models fuzzing as employed in [1]. The limitations of (a) and (b) have already been discussed in Section 2 and 3. Assumption (c) could be questionable in view of the following fact: the exact shape of the source and the sink of the correlator, i.e., the fuzzing or smearing prescription, is irrelevant only as long as there is sufficiently large overlap with the wavefunction of the state the mass of which is to be measured. This holds in general only for bound states. In our case, however, the correlator is supposed to be given by the exchange of two independently propagating, dressed gluons. We have already shown (cf. Figs. 4b,c, and 5a) that in this case the correlator is very sensitive to the chosen smearing (fuzzing) prescription.

However, assuming the validity of our assumptions, it is surprising that on the average the local masses $\mu(z)$ in the case $\pi_T = 0$ are close to the value obtained in [1] for the magnetic correlator ! In order to get the value of $\mu(z)a \approx 1.45$ at $z/a = 3$ (which was considered to give the best estimate for the mass determining the decay of the magnetic correlator in [1]), we have to assume π_T to be at most of the order of $(2\,T)^2$ (cf. Fig. 5b). On the average, $\pi_T \approx T^2$ (corresponding to $\mu_{real}a = 0.5$) can be best reconciled with the data of [1]. This, in turn, means that the local masses may easily overestimate the real masses by at least a factor of two.

However, a more detailed comparison of our results with the lattice data reveals further problems with this interpretation. In our calculation, the general behavior of the local masses still reflects the remnant enhancement at small z, giving rise to larger $\mu(z)$ at small z. This trend is not seen in the lattice data and could indicate that our form factor ansatz does not accurately model fuzzing as employed in [1]. We suggest that a lattice test of the dependence of the local masses on the level of fuzzing could help in clarifying the situation.

On the other hand, if our fuzzing model works accurately, we are lead to the conclusion that either the plaquette correlators may not be approximated by energy density correlators or that the latter are not dominated by the two–gluon exchange graph of Fig. 1d. If the first

possibility is true, then finite size effects are still too large to allow for a simple interpretation of the results of [1] in terms of continuum physics. In the second case, a continuum analysis which improves and corrects the simple picture investigated in the present work will be extremely difficult, since one does not a priori know which multi–gluon exchange diagrams yield the dominant contribution to the energy density correlators. However, in view of recent measurements of the spatial string tension [41] one might speculate that the magnetic correlator is dominated by a bound state, as represented by Fig. 1e. To confirm this, however, would require lattice data with much better statistics which is extremely difficult to obtain for the plaquette operators studied in [1]. In any case, if this picture is true, the interpretation of the screening mass extracted from the decay of the magnetic correlator as twice the gluon magnetic screening mass is not possible. Moreover, this indicates the breakdown of the simple perturbative picture of the gluon plasma, in accordance with the conclusions of [15].

Finally we comment on the electric correlator. Given the fact that in the continuum it is not very different from the magnetic, we may use (52) as a rough approximation also for the electric correlator. However, in that case the smaller local electric masses found in [1] ($ma \approx 0.8$, cf. Fig. 5b), can only be accounted for in our model by assuming that the actual electric screening mass is essentially zero! This would be in clear contradiction to the screening mass extracted from Polyakov–loop correlations [1] (unless they also suffer from ambiguities).

We conclude that independent measurements of especially the non–perturbative magnetic screening mass are needed to better pin down this physically interesting and phenomenologically relevant quantity [20].

Acknowledgments

We thank R.D. Pisarski for bringing this problem to our attention and T. Biro, G. Boyd, N. Christ, F. Karsch, V. Koch, R. Mawhinney, A. Schäfer, and M. Thoma for stimulating discussions. We are also indebted to U. Heller, F. Karsch, and R. Mawhinney for a critical reading of the final version of the manuscript and helpful comments.

References

[1] B. Grossmann, S. Gupta, U.M. Heller, F. Karsch, Nucl. Phys. B417 (1994) 289.

[2] Proceedings of Quark Matter 93, eds. E. Stenlund et al., Nucl. Phys. A566 (1994).

[3] H. Stöcker and W. Greiner, Phys. Rep. 137 (1986) 277.

[4] A.V. Selikhov and M. Gyulassy, Phys. Lett. B316 (1993) 373; Phys. Rev. C49 (1994) 1726.

[5] A.K. Rebhan, Phys. Rev. D48 (1993) R3967.

[6] H.A. Weldon, Phys. Rev. D26 (1982) 1394.

[7] D.J. Gross, R.D. Pisarski, L.G. Yaffe, Rev. Mod. Phys. 53 (1981) 43.

[8] K.J. Eskola and M. Gyulassy, Phys. Rev. C47 (1993) 2329.

[9] N.H. Christ, Nucl. Phys. A544 (1992) 81c.

[10] F. Karsch and H.W. Wyld, Phys. Lett. B213 (1988) 505.

[11] S. Gottlieb et al., Nucl. Phys. A498 (1989) 435c.

[12] K. Born et al., Phys. Rev. Lett. 67 (1991) 302.

[13] J. Engels, J. Fingberg, F. Karsch, D. Miller, M. Weber, Phys. Lett. B252 (1990) 625.

[14] J.B. Kogut and D.K. Sinclair, Nucl. Phys. B344 (1990) 238.

[15] D.H. Rischke, M.I. Gorenstein, A. Schäfer, H. Stöcker, W. Greiner, Phys. Lett. B278 (1992) 19;
D.H. Rischke, J. Schaffner, M.I. Gorenstein, A. Schäfer, H. Stöcker, W. Greiner, Z. Phys. C56 (1992) 325.

[16] V. Koch, E.V. Shuryak, G.E. Brown, A.D. Jackson, Phys. Rev. D46 (1992) 3169;
V. Koch, Phys. Rev. D49 (1994) 6063.

[17] S. Chapman, Phys. Rev. C47 (1993) 1763;
A. Gocksch and R.D. Pisarski, Nucl. Phys. B402 (1993) 657.

[18] see also: B. Berg, A. Billoire, Nucl. Phys. B221 (1983) 109.

[19] M. Teper, Phys. Lett. B183 (1986) 345.

[20] Such investigations are presently performed at the University of Bielefeld (G. Boyd, F. Karsch, private communication).

[21] V.V. Klimov, Sov. Phys. JETP 33 (1981) 934.

[22] for a review, see: E.V. Shuryak, Rev. Mod. Phys. 65 (1993) 1.

[23] The bare mass is even smaller and can be completely neglected for this consideration.

[24] V.L. Eletskii and B.L. Ioffe, Sov. J. Nucl. Phys. 48 (1988) 384;
W. Florkowski and B.L. Friman, Z. Phys. A347 (1994) 271.

[25] A. Gocksch, Phys. Rev. Lett. 67 (1991) 1701.

[26] T. Schäfer, E.V. Shuryak, J.J.M. Verbaarschot, preprint SUNY–NTG–94–24, State University of New York at Stony Brook, 1994.

[27] This, however, can be done studying the quark propagator itself, see: G. Boyd, S. Gupta, F. Karsch, Nucl. Phys. B385 (1992) 481.

[28] see, for instance: M. Creutz, "Quarks, gluons and lattices", Cambridge University Press, Cambridge, 1983.

[29] The actual lowest order term is trivial ($= 1/2$) and cancels when the *connected* correlator is considered.

[30] J. Glimm, A. Jaffe, "Quantum Physics, A Functional Integral Point of View", Springer, New York, 1987.

[31] I.S. Gradsteyn, I.M. Ryzhik, "Table of Integrals, Series, and Products", eq. (3.354.5), Academic Press, San Diego, 1980.

[32] I.S. Gradsteyn, I.M. Ryzhik, "Table of Integrals, Series, and Products", eqs. (3.351.2), (3.352.2), and (8.212.3), Academic Press, San Diego, 1980.

[33] J.I. Kapusta, "Finite–temperature field theory", Cambridge University Press, Cambridge, 1989.

[34] E. Braaten and R.D. Pisarski, Nucl. Phys. B337 (1990) 569.

[35] I.S. Gradsteyn, I.M. Ryzhik, "Table of Integrals, Series, and Products", eq. (3.728.1), Academic Press, San Diego, 1980.

[36] F. Karsch, private communication.

[37] B.E. Baaquie, Phys. Rev. D16 (1977) 2612;
U. Heller and F. Karsch, Nucl. Phys. B251 [FS13] (1985) 254.

[38] H.–Th. Elze, K. Kajantie, J. Kapusta, Nucl. Phys. B304 (1988) 832.

[39] L. Fernandez and E. Marinari, Nucl. Phys. B295 (1988) 51;
C. Michael and M. Teper, Nucl. Phys. B340 (1989) 347.

[40] I.S. Gradsteyn, I.M. Ryzhik, "Table of Integrals, Series, and Products", eq. (1.341.3), Academic Press, San Diego, 1980.

[41] G.S. Bali, J. Fingberg, U.M. Heller, F. Karsch, K. Schilling, Phys. Rev. Lett. 71 (1993) 3059.

Figure Captions:

Fig. 1: Topologically distinct graphs contributing to the energy density correlator: (a) one–loop, two–gluon exchange diagram with free gluon propagators, (b,c) two– and three–loop diagrams with free gluon propagators, (d) one–loop, two–gluon exchange diagram with dressed gluon propagators, (e) generic ladder diagram representing propagation of a bound gluon pair, and (f) one–loop, two–gluon exchange with smeared source and sink.

Fig. 2: (a) The magnetic correlator in the interaction–free case normalized to T^5 as a function of zT (full line) and the contribution of the zero Matsubara mode (dotted line). (b) The normalized magnetic (dotted curve) and electric correlator (full line) as functions of zT.

Fig. 3: (a) The magnetic (short–dashed curve) and electric correlator (long–dashed curve) for $\pi_L = (1.4\,T)^2$ and $\pi_T = (2.9\,T)^2$ in comparison to the interaction–free result of Fig. 2b. (b) Different contributions to the electric correlator: the dotted curve corresponds to the contribution of the zero mode, while the full line represents the full result. The exponentially damped terms with $n \neq 0$ constitute the difference between these curves at small zT, the anomalous polynomially decaying term the difference for large zT.

Fig. 4: (a) The magnetic correlator for the interaction–free case in the continuum (long–dashed curve: $\pi_T = 0$, dotted curve: $\pi_T = (2.9\,T)^2$) in comparison to a calculation on a 4×16^3–lattice (squares: $m = 0$, circles: $m = 2.9\,T$). (b) The magnetic correlator on the lattice for $m = 2.9\,T$ and different degrees of smearing. The solid curve corresponds to point sources and sinks ($L_\sigma = L_\tau = 0$), the dashed curve to smearing with $L_\sigma = L_\tau = 1$, the dashed–dotted curve to $L_\sigma = L_\tau = 2$, the long–dashed curve to $L_\sigma = 4$, $L_\tau = 2$, and the dotted curve to $L_\sigma = 8$, $L_\tau = 2$. (c) The same as in (b) for $m = 0$.

Fig. 5: (a) Local masses extracted via (54) from the magnetic correlators of Figs. 4b,c. The upper set of curves is for $m = 2.9\,T$, the lower for $m = 0$. (b) Local masses extracted from the magnetic correlator with maximal smearing ($L_\sigma = 8$, $L_\tau = 2$). The curves are labelled with the real gluon mass entering the calculation of the correlator. Black squares are local masses extracted from data [1] for the magnetic correlator, open circles are local masses corresponding to the electric correlator.

Fig. 1

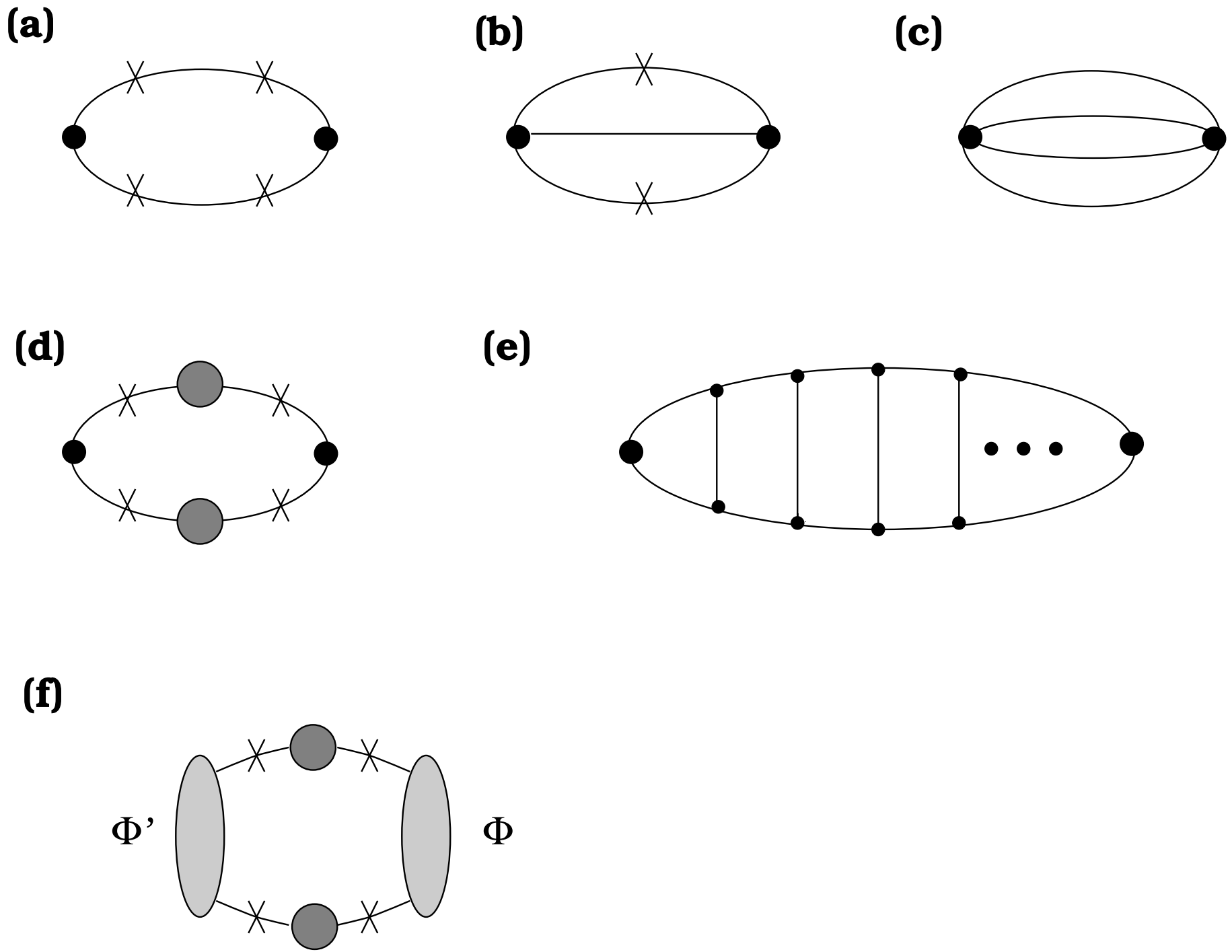

This figure "fig1-1.png" is available in "png" format from:

http://arXiv.org/ps/nucl-th/9409006v1

This figure "fig2-1.png" is available in "png" format from:

http://arXiv.org/ps/nucl-th/9409006v1

Fig. 2a

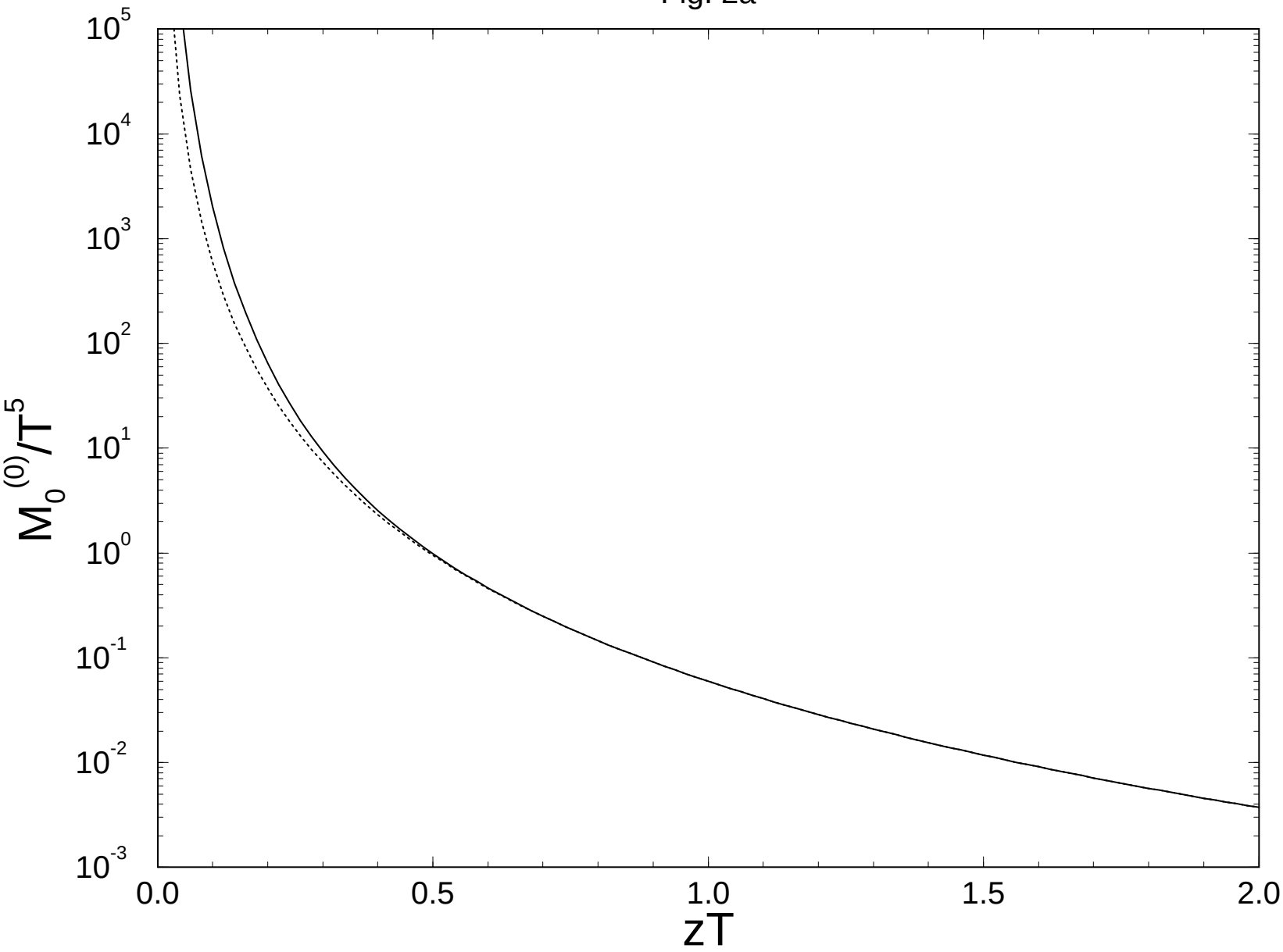

Fig. 2b

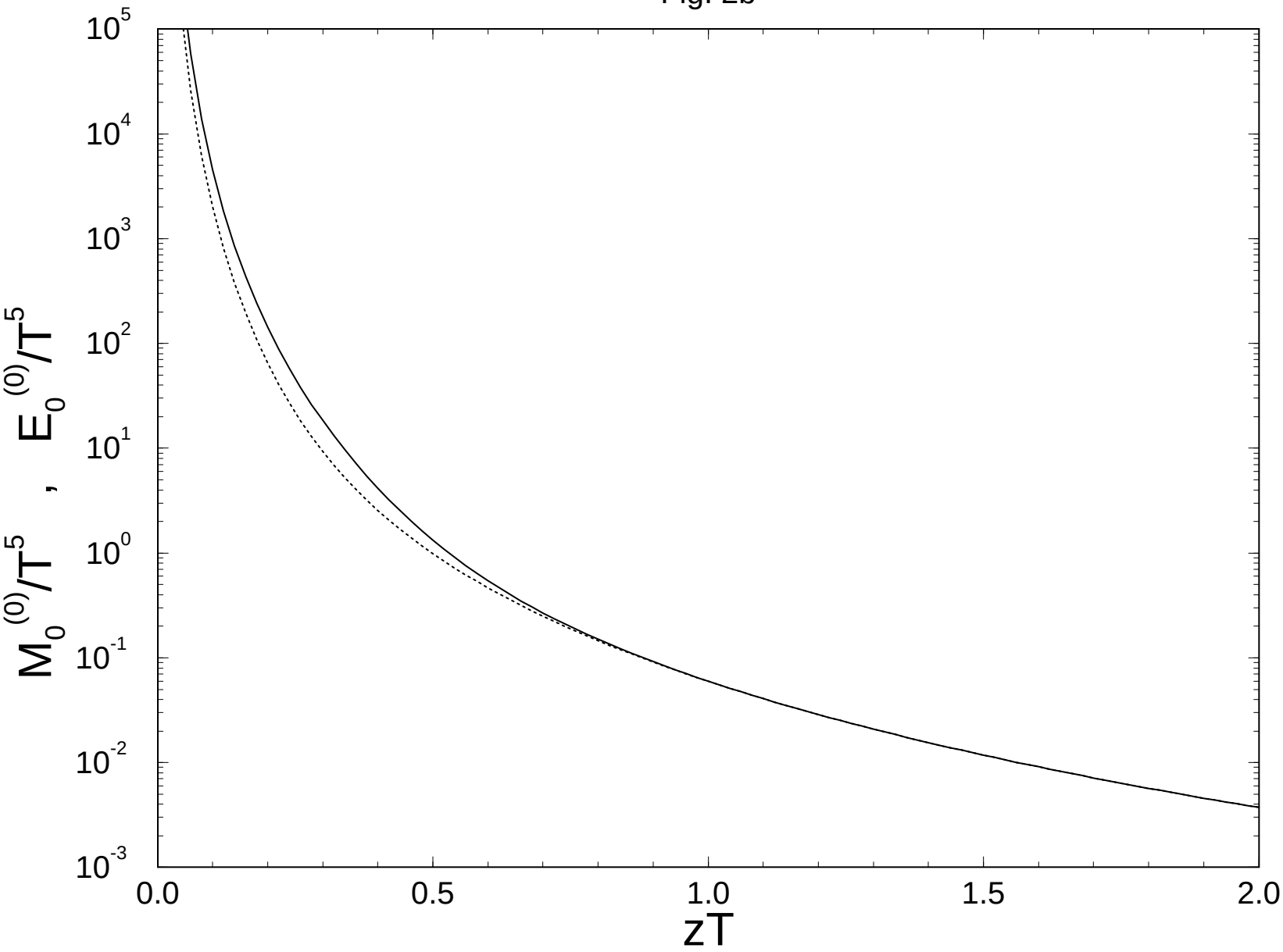

This figure "fig1-2.png" is available in "png" format from:

http://arXiv.org/ps/nucl-th/9409006v1

This figure "fig2-2.png" is available in "png" format from:

http://arXiv.org/ps/nucl-th/9409006v1

Fig. 3a

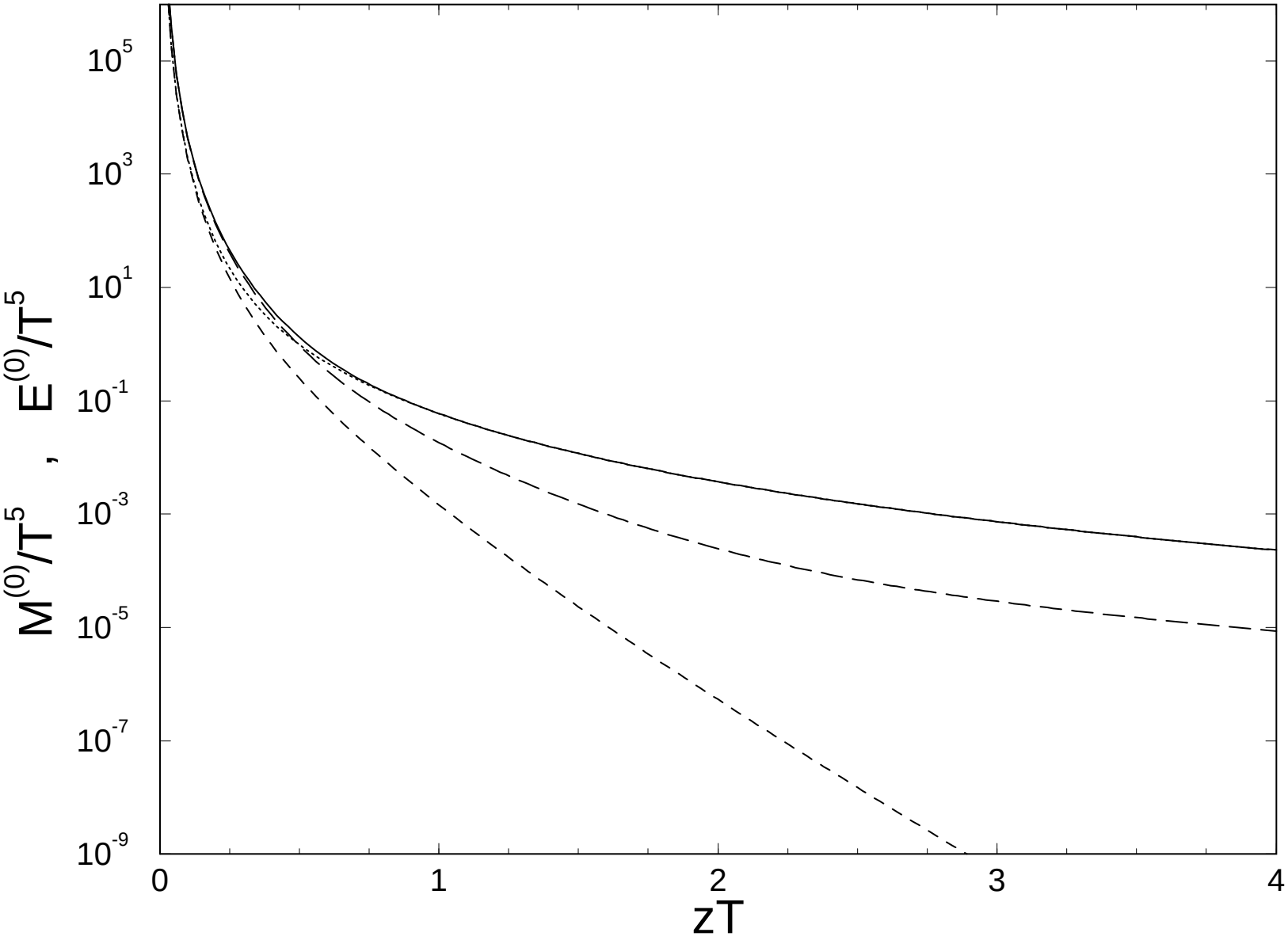

Fig. 3b

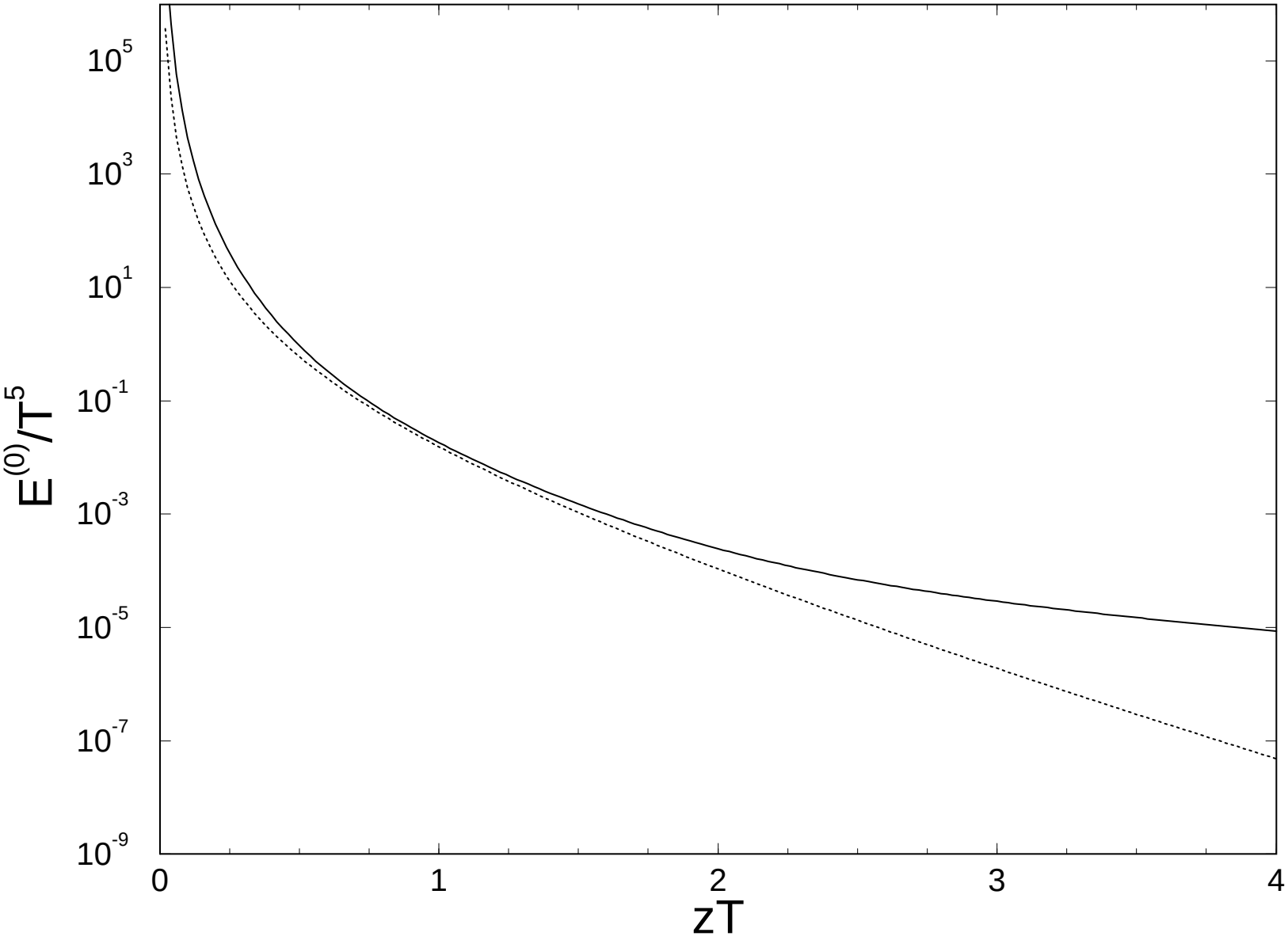

This figure "fig1-3.png" is available in "png" format from:

http://arXiv.org/ps/nucl-th/9409006v1

This figure "fig2-3.png" is available in "png" format from:

http://arXiv.org/ps/nucl-th/9409006v1

Fig. 4a

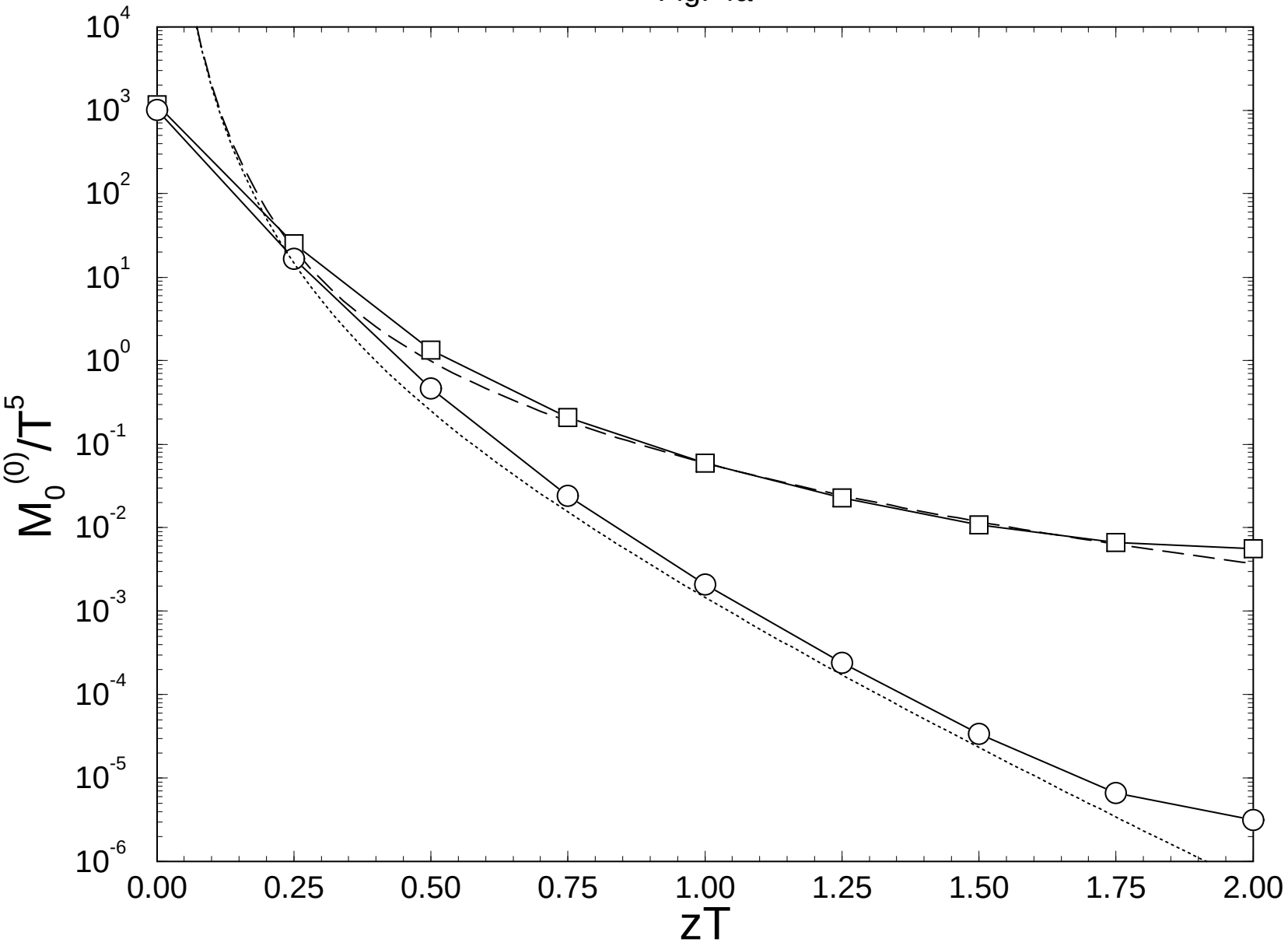
10^4
10^3
10^2
10^1
10^0
10^{-1}
10^{-2}
10^{-3}
10^{-4}
10^{-5}
10^{-6}
$M_0^{(0)}/T^5$
0.00
0.25
0.50
0.75
1.00
1.25
1.50
1.75
2.00
zT

Fig. 4b

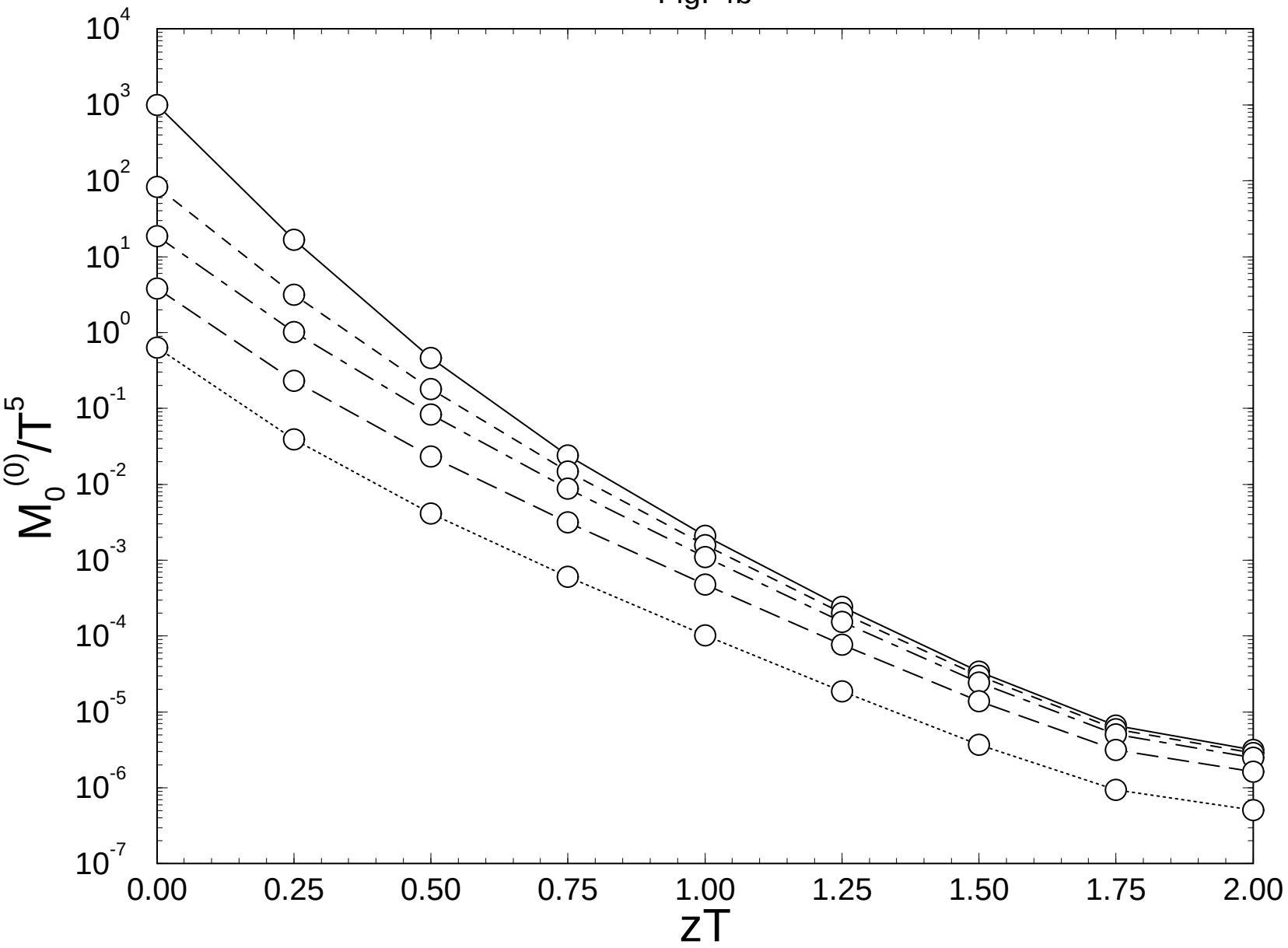
10^4
10^3
10^2
10^1
10^0
10^{-1}
10^{-2}
10^{-3}
10^{-4}
10^{-5}
10^{-6}
10^{-7}
$M_0^{(0)}/T^5$
0.00
0.25
0.50
0.75
1.00
1.25
1.50
1.75
2.00
zT

Fig. 4c

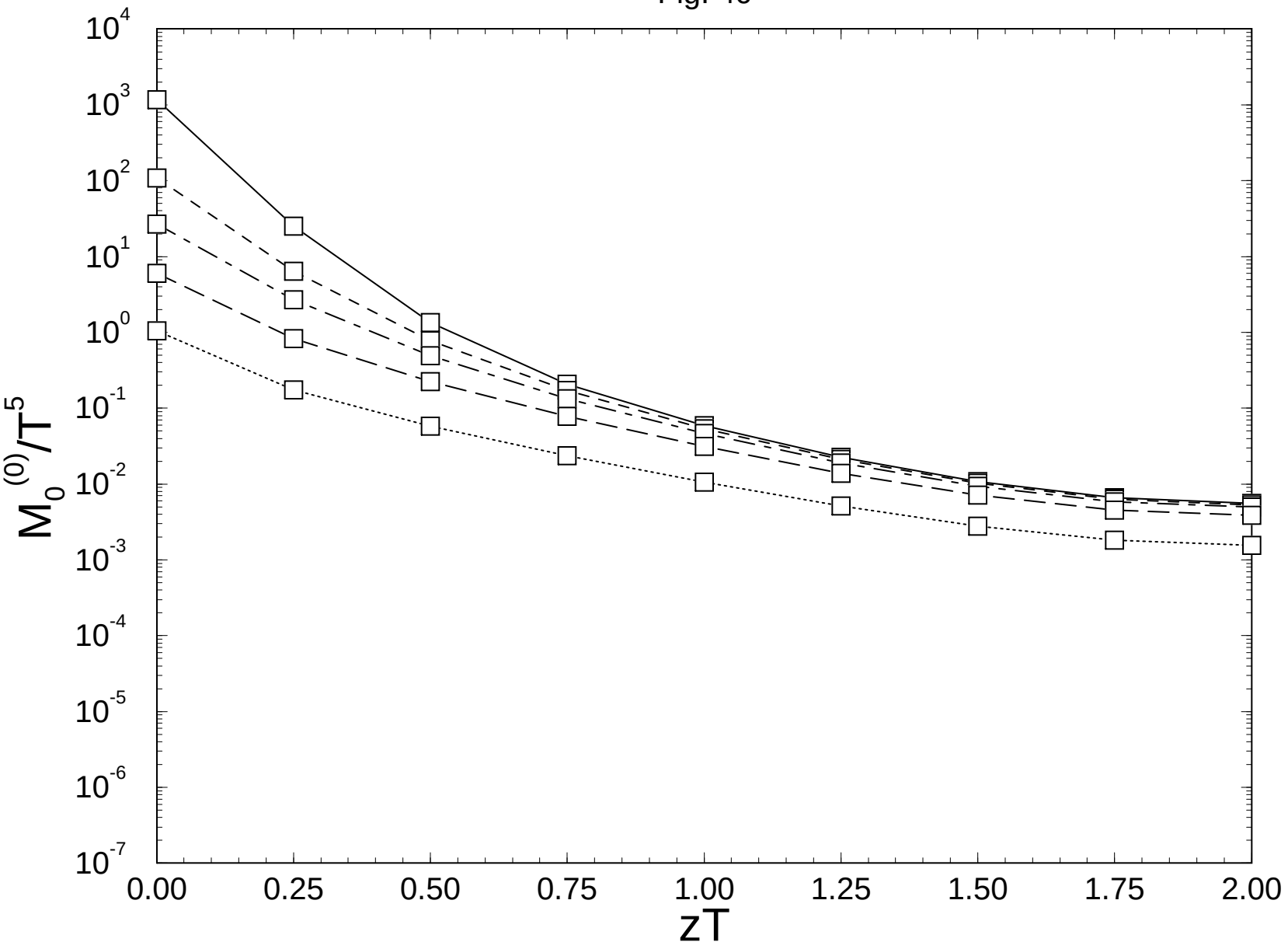
10^4
10^3
10^2
10^1
10^0
10^{-1}
10^{-2}
10^{-3}
10^{-4}
10^{-5}
10^{-6}
10^{-7}
$M_0^{(0)}/T^5$
0.00
0.25
0.50
0.75
1.00
1.25
1.50
1.75
2.00
zT

This figure "fig1-4.png" is available in "png" format from:

http://arXiv.org/ps/nucl-th/9409006v1

This figure "fig2-4.png" is available in "png" format from:

http://arXiv.org/ps/nucl-th/9409006v1

Fig. 5a

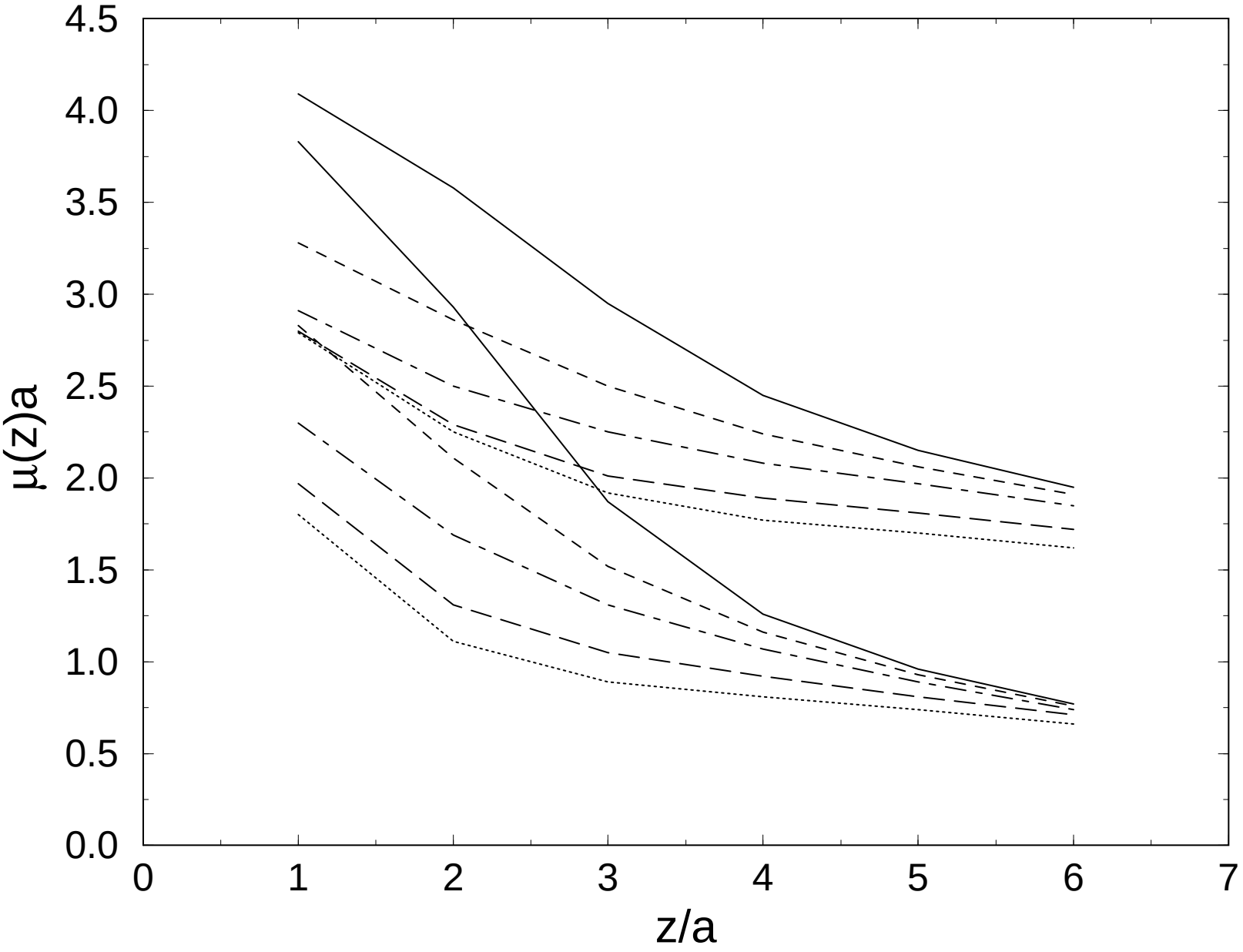

Fig. 5b

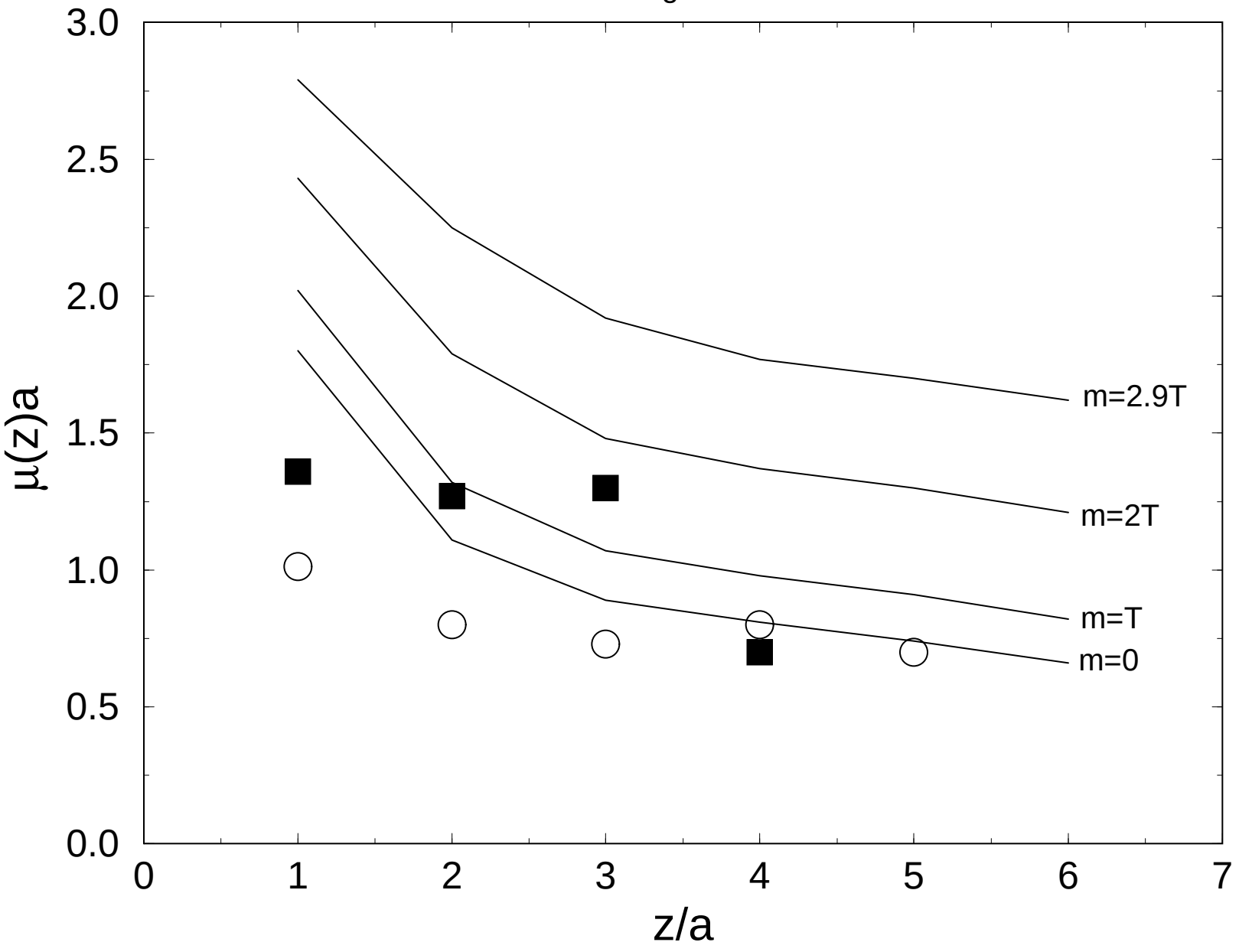

This figure "fig1-5.png" is available in "png" format from:

http://arXiv.org/ps/nucl-th/9409006v1

This figure "fig2-5.png" is available in "png" format from:

http://arXiv.org/ps/nucl-th/9409006v1